

Demixing of Binary Water–Chloroform Mixtures Containing Ionophoric Solutes and Ion Recognition at a Liquid–Liquid Interface: A Molecular Dynamics Study

N. Muzet, E. Engler, and G. Wipff*

Laboratoire MSM, UMR 7551, Institut de Chimie, Université Louis Pasteur, 4 rue B. Pascal, 67 000 Strasbourg, France

Received: April 15, 1998

We report a series of molecular dynamics simulations on the demixing of “homogeneous” binary water–chloroform mixtures containing species involved in the assisted ion extraction process. We consider an ionophore **L** (**L** = 1,3-alternate calix4arene-crown6), uncomplexed salts of Cs^+ and the LCs^+ and LNa^+ cation complexes with a lipophilic (Pic^-) and a hydrophilic (Cl^-) counterion, respectively, as being solutes. In all cases, the liquids separate rapidly, leading to two solvent slabs separated by a well-defined interface. However, the final state is very different, depending on the hydrophilic/hydrophobic balance of the solutes: the Cs^+ and NO_3^- ions of the CsNO_3 salt are completely immersed in the aqueous phase, whereas Pic^- anions display a strong adsorption at the interface. The LCs^+ complex and the free ligand **L**, although more soluble in the organic phase than in water, also display a surfactant like behavior. Similar conclusions are obtained when **L**, LCs^+ , Cs^+ Pic^- , and Cs^+ NO_3^- ions are simultaneously present in the solution. On the basis of free energy perturbation calculations on LM^+ complexes, we calculate a marked Cs^+/Na^+ recognition by **L** at the interface. These results have important implications concerning the mechanism of ionophore assisted liquid–liquid ion extraction and recognition processes at the interface.

I. Introduction

Ions complexed by ionophores can be extracted from an aqueous to an organic phase. The extraction experiment generally proceeds by mixing an aqueous solution of the salts with an organic solution of the water insoluble extractant molecule (“ionophore”).^{1,2} Mixing is achieved mechanically by shaking the whole system. Then, phase separation takes place, due to gravitational forces or centrifugation, and differences in surface tension between the two liquids. At some stage, the cation is captured by the ionophore and extracted into the organic phase. The precise mechanism of ion capture and extraction is still unknown but it is stressed that the interfacial region between water and the organic solvent plays a crucial role.^{1,3,4} The nature of the metastable mixed phase is ill-defined, as it may range from a perfectly mixed homogeneous system to droplets or microemulsions involving the two liquid systems.

This paper reports a theoretical study on the demixing of different “perfectly mixed” water–chloroform binary solutions containing typical solutes involved in the liquid–liquid extraction process, with a particular focus on the phase separation, and on the precise solvation and location of the solutes. As solutes we consider an ionophore **L** (**L** = 1,3-dimethoxycalix-4-arene-crown-6; see Chart 1), in its free and complexed LM^+ states ($\text{M}^+ = \text{Cs}^+/\text{Na}^+$), and a M^+ cation also free and complexed, with different counterions. **L** and 1,3-alternate calixarene analogues belong to a new class of extractant molecules for Cs^+ ions.^{5–7} The Cs^+/Na^+ selectivity, observed in the liquid–liquid water–chloroform system, as well as in supported liquid membranes systems, is of high interest in the context of Cs^+ decontamination from nuclear wastes.^{8–10}

More specifically, we simulated the demixing of neat binary solutions and of solutions containing the inclusion complex LCs^+ , with Cl^-/Pic^- as counterions. Pic^- , widely used in extraction experiments due to its lipophilic character and

CHART 1: The LM^+ Complex

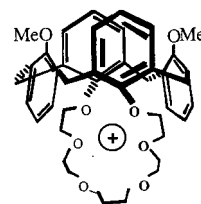
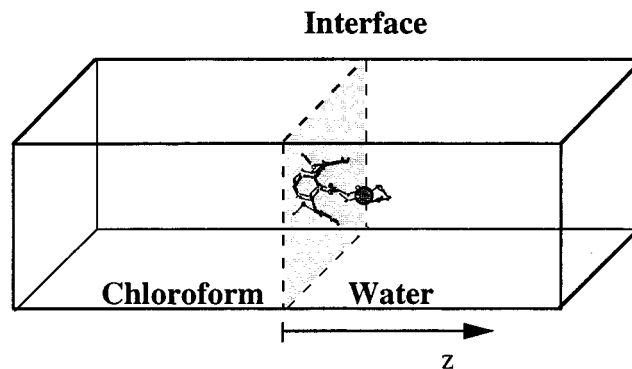


CHART 2: Representation of the Simulation Box, with the Two Liquid Phases after Full Phase Separation



spectroscopic properties, was compared to the more hydrophilic Cl^- counterion. We also considered the LNa^+Pic^- complex as a solute. Because the Na^+ cation is not extracted by **L**, it was indeed important to test whether LNa^+ remains of an inclusive type during the demixing simulation. A second series of simulations dealt with binary solutions of uncomplexed salts, $(\text{Cs}^+\text{Pic}^-)_4$ and $(\text{Cs}^+\text{NO}_3^-)_4$, respectively, about 4 times more concentrated than the LM^+ complexes (Table 1). NO_3^- was chosen as counterion because it is present at high concentration in liquid solutions containing nuclear waste, since it results from

TABLE 1: Simulation Conditions

solute		box size (Å ³)	solvent ^a N _{chl} + N _{wat}	cut off (Å)	demixing time (ps) ^b	total time (ps) ^c
no solute	A	35 × 35 × 79	373 + 1645	12	400	700
LCs ⁺ Cl ⁻	B	39 × 35 × 65	304 + 1504	12	400	450
LCs ⁺ Cl ⁻	C	39 × 35 × 65	307 + 1504	12	300	375
LCs ⁺ Cl ⁻	C'	39 × 35 × 65	307 + 1504	12	350	450
LCs ⁺ Pic ⁻	D	42 × 38 × 61	363 + 1564	12	400	675
LCs ⁺ Pic ⁻ pol ^d		42 × 38 × 61	363 + 1564	12	550	670
LNa ⁺ Pic ⁻	E	42 × 38 × 61	363 + 1564	12	500	870
(Cs ⁺ Pic ⁻) ₄	F	42 × 38 × 58	339 + 1534	12	350	1000
(Cs ⁺ Pic ⁻) ₄	G	42 × 38 × 58	339 + 1534	12	375	675
(Cs ⁺ Pic ⁻) ₄ Ewald ^e		42 × 38 × 58	339 + 1534	12	425	500
(Cs ⁺ NO ₃ ⁻) ₄	H	34 × 40 × 61	291 + 1452	12	425	600
mixture 1 ^f	I	39 × 43 × 74	446 + 1846	12	650	1000
mixture 2 ^g	J	39 × 43 × 74	446 + 1846	12	780	1000
no solute ^h	K ₁	30 × 30 × 50	166 + 754	13.5	410	475
no solute ^h	K ₂	30 × 30 × 50	166 + 754	13.5	375	475
no solute ^h	K ₃	30 × 30 × 50	166 + 754	13.5	375	475

^a Number of chloroform and water molecules. ^b Time after which complete phase separation has taken place. ^c Total time simulated for the demixing experiment. ^d Simulation with the “polar” model of chloroform. ^e Simulation with the Ewald summation. ^f See text for definition. ^g See text for definition. ^h Simulations K₁ to K₃ with three different chloroform models (see text).

the dissolution of the metals by nitric acid. The last series of simulations concerned more “realistic” and complex mixtures, containing simultaneously **L** (either free or complexed with Cs⁺), the Cs⁺Pic⁻, and the Cs⁺NO₃⁻ salts. They were compared with solutions of single solute(s).

It is of primary interest to obtain microscopic views of the demixing process, with the following questions in mind. How fast and effective is the liquid phases separation? Does it depend on the nature of the solute? Will the **LM**⁺ complex sit in the organic phase where it is known to be extracted? Will uncomplexed salts M⁺ X⁻ sit in the aqueous phase where they are more soluble? In relation to the question of extraction selectivity, it is also important to compare the complexes of a cation known to be extracted (Cs⁺), with a hypothetical one which is not (Na⁺). Another important question concerns the role of the counterion in the cation extraction process. In particular, whether the Pic⁻ anions facilitate the extraction of the complex, as anticipated from experiment.

In this paper, we also address the crucial question of ion recognition in liquid–liquid extraction and, on the basis of free energy (FEP) calculations, we consider the Na⁺/Cs⁺ binding by **L** at the liquid–liquid interface.

II. Methods

1. Energy Representation of the System. We used the modified AMBER4.1 software¹¹ with the following representation of the potential energy:

$$U = \sum_{\text{bonds}} K_r (r - r_{\text{eq}})^2 + \sum_{\text{angles}} K_\theta (\theta - \theta_{\text{eq}})^2 + \sum_{\text{dihedrals}} \sum_n V_n (1 + \cos n\phi) + \sum_{i < j} (q_i q_j / R_{ij} - 2\epsilon_{ij} (R_{ij}^*/R_{ij})^6 + \epsilon_{ij} (R_{ij}^*/R_{ij})^{12})$$

The bonds and bond angles were treated as harmonic springs and a torsional term was associated with the dihedral angles. The interactions between atoms separated by at least three bonds were described by a pairwise additive 1–6–12 potential. Parameters for the solutes were taken from the AMBER force field¹² and from previous studies of these molecules in pure homogeneous solvents.^{13,14} The atomic charges on **L**^{13,14} and on the Pic⁻ anion¹⁵ were derived from electrostatic potentials. The Na⁺ to Cs⁺ alkali cations were described by the Åqvist parameters.¹⁶ For the solvent, we used the TIP3P model for water¹⁷ and the OPLS model for chloroform¹⁸ where CH is

represented in the united atom approximation. For the van der Waals interactions between unlike atoms, the R_{ij}^* and ϵ_{ij} parameters were calculated using the Berthelot–Lorentz combination rules: $R_{ij}^* = R_i^* + R_j^*$ and $\epsilon_{ij} = (\epsilon_i \epsilon_j)^{1/2}$. A residue based cutoff of 12 Å was used for the nonbonded interactions.

The MD simulations were started with random velocities, and the temperature was controlled by coupling to a thermal bath¹⁹ with a relaxation time of 0.2 ps. All C–H, O–H, H···H, C–Cl, and Cl···Cl “bonds” were constrained with SHAKE, using a time step of 1 fs.

Additional tests were performed concerning the representation of the chloroform solvent. First, we used the united atom model with OPLS charges scaled by 1.3, to mimic a “polarized” solvent. Second, we used an all atom model, in conjunction with explicit polarization, taken from ref 20. Furthermore, to investigate the possible effect of long-range electrostatic interactions on the demixing process, the demixing of the (Cs⁺Pic⁻)₄ solution was simulated with the particle mesh Ewald summation method,²¹ as implemented in AMBER4.1, using the standard OPLS model for chloroform and 12 Å cutoff distance.

2. Solvent System. The biphasic mixed solutions were built independently for each system. In each case, the mixed binary water–chloroform solution was prepared stepwise, starting from two adjacent cubic boxes of pure liquids, of about 40 × 40 × 30 Å³ each, containing 300–370 chloroform and 1300–1600 water molecules. Details are given in Table 1. After immersion of the solute near the interface, each system was energy minimized and equilibrated at 300 K under a constant pressure of 1 atm, to ensure that both liquid phases approach their correct densities (of 1.0 and 1.47, respectively) “in the bulk regions”. The mixing of the system was speeded up by scaling up the chloroform charges by 4.0 and by running 400–900 ps of MD at 500 K at constant volume. This was followed by the demixing simulations, performed at 300 K and constant volume, with charges on chloroform reset to their OPLS values ($q_C = 0.42$ and $q_{Cl} = -0.14$). Each demixing simulation was run until complete phase separation was observed (about 0.4–1 ns).

As the outcome of the demixing may depend on the starting configurations, we considered different starting states in some cases.

3. Binding Selectivity: Free Energy Calculations. The change in free energy between two states (ions M₁⁺ and M₀⁺) was calculated by using the statistical perturbation theory, using the windowing technique.¹¹ The potential energy was defined

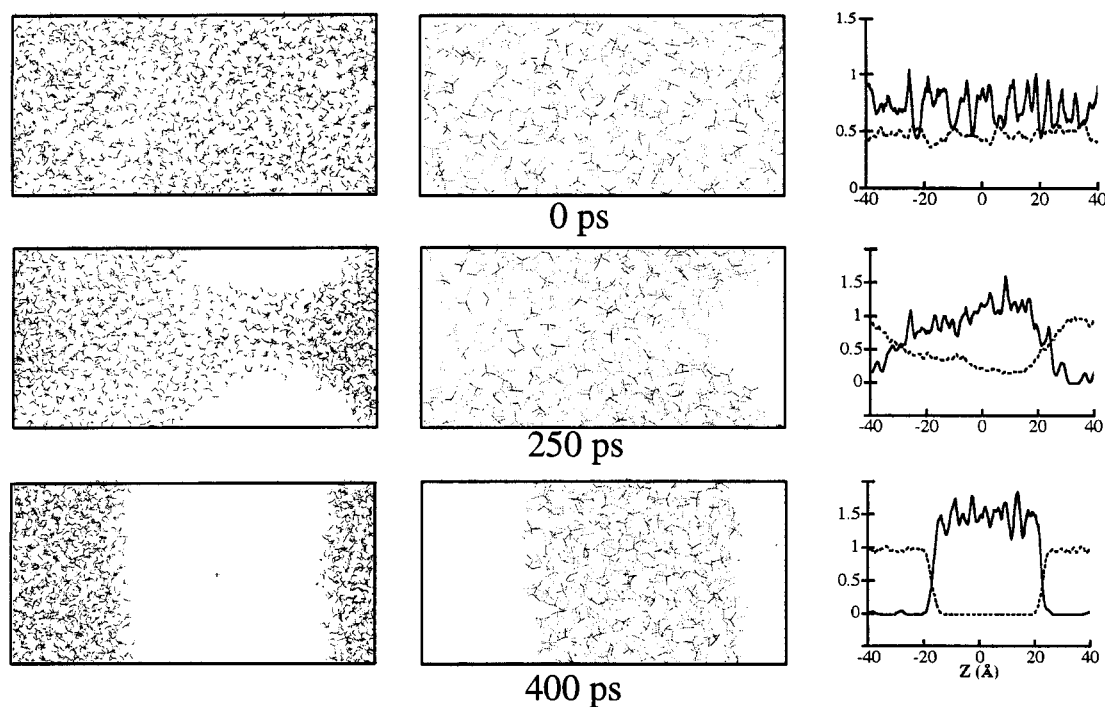


Figure 1. Demixing simulation (A) of the binary water–chloroform solution (no solute). Snapshots at 0, 250, and 400 ps, showing the water solvent only (left) or the chloroform only (middle). The density curves of the solvents (chloroform, full line; water, dotted line) as a function of Z (defined in Chart 1) are shown right.

as $U_\lambda = \lambda U_1 + (1 - \lambda)U_0$, where U_1 and U_0 were calculated with the corresponding R_1^* , ϵ_1 and R_0^* , ϵ_0 parameters of the ions. At each window, the difference in free energy between the states λ and $\lambda + \Delta\lambda$ (“forward calculation”) and between the states λ and $\lambda - \Delta\lambda$ (“backward calculation”) was obtained by

$$\Delta G_{\lambda_i} = G_{\lambda_{i+1}} - G_{\lambda_i} = -RT \ln \left\langle \exp - \frac{U_{\lambda_{i+1}} - U_{\lambda_i}}{RT} \right\rangle_{\lambda_i}$$

where R is the molar gas constant and T is the absolute temperature. $\langle \rangle$ stands for the ensemble average at the state λ_i where U_{λ_i} is the potential energy. At each window, 2 ps of equilibration were followed by 3 ps of MD for data collection and averaging. Additional tests were performed with enhanced sampling (4 + 6 ps) at each window for the $\text{LNa}^+/\text{LCs}^+$ mutations and 4 + 16 ps for the LNa^+/LK^+ mutations. Details are given in the text and in Table 2.

4. Analysis of Results. The results were analyzed from the atom trajectories which were saved every 0.5 ps. The position of the interface between the two liquid phases was recalculated at each step and defined as in ref 22 by the intersection between the density curves of the two liquids.

To follow the phase separation as a function of time, we defined a “demixing index” χ_{demix} , calculated as follows from each set of coordinates. The whole volume was split into n cubic boxes (n ranges from about 60 to 100) of about 10 Å in width. In each box, we calculated the densities of water ($d_{\text{wat},i}$) and of chloroform ($d_{\text{chlor},i}$), and $1/d_i = 1/d_{\text{wat},i} + 1/d_{\text{chlor},i}$. To avoid edge effects, the calculation was repeated with two sets of boxes, whose centers were shifted by 5 Å. The “demixing index” was obtained from the average over all boxes of the two sets ($\chi_{\text{demix}} = \langle d_i \rangle$) and normalized in such a way that χ_{demix} ranges from 1.0 (for a perfectly mixed homogeneous system) to 0.0 (for two nonoverlapping separated phases).

III. Results

The simulations are labeled A to K (Table 1). In all cases, phase separation was rapid, leading in about 500 ps or less to adjacent liquid slabs, separated by a nearly flat interface. In the following, we first describe the demixing of the “neat” binary solution (A, section 1), and the demixing of solutions containing a single solute: the complexed ionophore (LCs^+Cl^- , LCs^+Pic^- , LNa^+Pic^-) (B–E; section 2). This is followed (F–H; section 3) by the results of the demixing of solutions containing uncomplexed salts of Cs^+ , with Pic^- and with NO_3^- as counterions, respectively. In section 4 (I and J), we consider mixtures containing simultaneously L , LCs^+Cl^- , Cs^+Pic^- , and Cs^+NO_3^- . The main events that occur during the “demixing experiments” and the final states are described, based on selected snapshots, where the two solvents are shown side by side, instead of superposed, for clarity. Section 5 deals with the question of Na^+/Cs^+ binding selectivity at the interface. The question of rate and driving forces for phase separation, relevance of the results regarding the mechanism of ion extraction, and computational aspects are presented in the discussion section.

1. Demixing Simulation A: The “Neat” Binary Water–Chloroform Solution. It can be seen in Figure 1 that, at 0 ps, the two liquids formed a quite homogeneous mixture. Their densities, plotted as a function of the Z dimension of the box, were about half of their values in the pure liquids (1.0 and 1.47, respectively). When the demixing simulation started (i.e., by turning T down to 300 K and resetting the charges on chloroform to their OPLS values), the two liquids separated rapidly, forming first small water clusters and, after 250 ps, two regions with high concentrations of water and chloroform, respectively (Figure 1). Notice that, due to the periodic boundary conditions, the “top” and the “bottom” of the box are in fact adjacent, and chloroform molecules are clustered inside a “pocket”. At that stage, there was still however some gradient

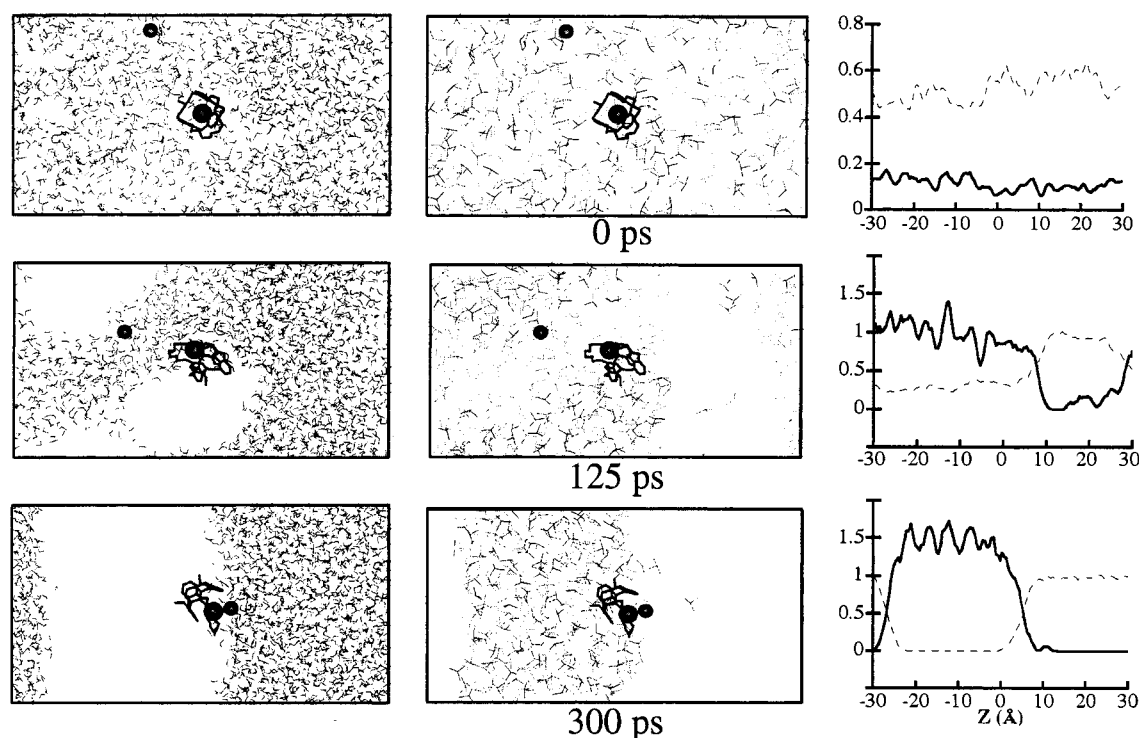


Figure 2. Demixing simulation (C) of the binary solution containing the LCs^+Cl^- complex (at 0, 125, and 300 ps). See Figure 1 for comments.

of solvent concentrations, and the two liquids somewhat were mixed at the boundaries of the pocket.

However, full separation of the two liquids proceeded further rapidly, leading to a chloroform slab, surrounded by two water slabs. The density of water in the water slab (Figure 1) was nearly constant at 1.0, while the density of chloroform in the chloroform slab was about 1.5, and displayed some fluctuations, as noticed in the simulations of the water–chloroform interface.²² The interfacial region was flat and narrow (of about 5–7 Å is width). We also noticed that the chloroform slab was completely dry, while the water slab contained one molecule of chloroform.

2. Demixing Simulations B – E: Binary Solutions of the LM^+X^- Complexes. In the early stages of these simulations, clustering of chloroform and of water could be observed (Figures 2 and 3). The organic molecules aggregated readily around the aromatic groups of **L**, water molecules aggregated around the complexed Cs^+ or Na^+ cations. The Cl^- counterions behaved differently from the Pic^- , as far as their solvent surrounding and relationship with the complexed cation was concerned. In all cases, the LM^+ cation complexes remained of inclusive type and **L** retained its 1,3-alternate conformation. Some details are given below, with a particular focus on the outcome of the process.

LCs^+Cl^- Solution. Three independent simulations were performed on this system, which differed by the initial relationship between Cl^- and the complexed Cs^+ . In simulation B, Cl^- was initially at 10 Å from the complexed Cs^+ , while in simulation C, it was at 23 Å (Figures 2 and S1 (for S1, see Supporting Information)). Demixing simulation C' started after an additional 100 ps of mixing time, compared to that of C, with Cl^- at 17 Å from LCs^+ . With the three starting situations, demixing took place readily, leading to nearly identical situations where LCs^+ adsorbed at the interface. However, in B and C, Cl^- was in intimate contact with Cl^- , while in C', the anion was captured by the bulk water phase and remote (15 to 20 Å) from LCs^+ (Figure S2 (see Supporting Information)). As

expected, the hydrophilic moieties of the solute (Cs^+ and the crown ether fragment of **L** and Cl^- in cases B and C) were finally on the water side of the interface, while the aromatic core of **L** was on the chloroform side. The density curves (Figures 2 and S1) confirm that the solvent phases reached densities close to the values of the pure liquids. The fact that Cl^- was not always captured by water and separated from LCs^+ is somewhat surprising, especially in simulation C where Cl^- was initially beyond the cutoff distance from Cs^+ . Computer graphics and energy component analysis suggest that this does not result, at the beginning, from the cation–anion attraction, but from the initial location of Cl^- and the water flow where it is more or less immersed. Indeed, the pattern of water phase formation in C (Figure 2; 125 ps) is such that Cl^- sits in a water “corridor” which links the two forming “bulk water” slabs (right-hand side of Figure 2). As this “corridor” disrupts (due to the solvent–solvent interactions; see discussion), Cl^- approaches close to LCs^+ enough to be attracted by Cs^+ . We checked that this demixing simulation C restarted at 140 ps (when the $\text{Cl}^- \cdots \text{Cs}^+$ distance is about 10 Å) with randomized velocities also led to this pair which remained intimate when the simulation was pushed up to 0.5 ns. On the other hand, we found that a simulation starting with LCs^+ at the interface and Cl^- in water at about 7 Å from Cs^+ did not lead to ion pairing but to diffusion of the anion in the water slab. Taken together, these results suggest that there is an energy barrier for ion pair formation/dissociation at the interface, which arises from the water stripping around the ions as they pair. At the early stages of demixing B and C, the local concentration of water around Cl^- and LCs^+ seems to be low enough to reduce this barrier.

LCs^+Pic^- (D) and LNa^+Pic^- (E) Solutions. A major difference of these systems, compared to the LCs^+Cl^- concerns the Pic^- anions, which remained, from the early stages until the end of the demixing, in contact with both water and chloroform molecules (Figure 3).

After 400 ps the two liquid phases were separated by a “flat” interface, where LCs^+ or LNa^+ adsorbed on the chloroform

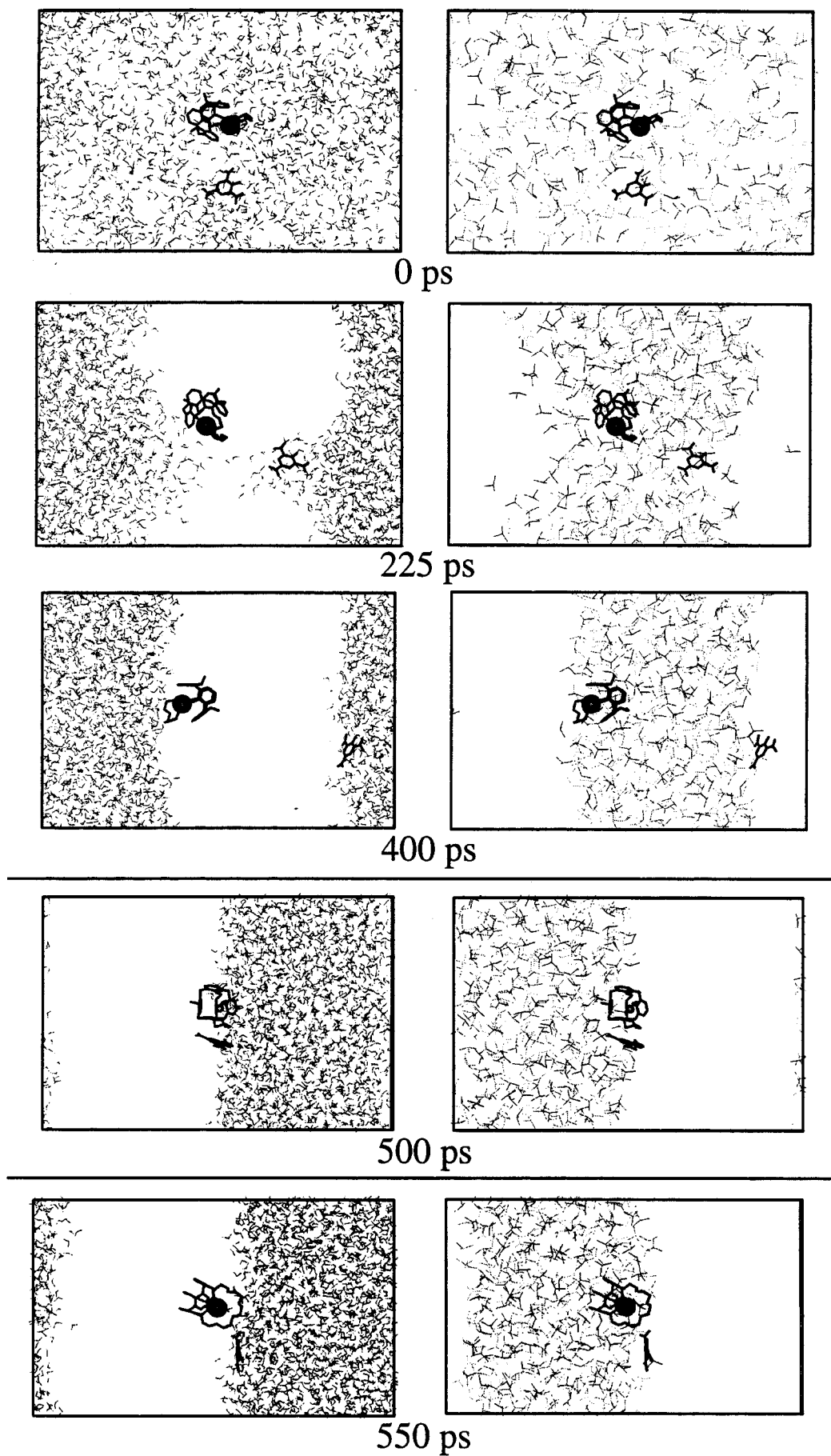


Figure 3. From top to bottom: Demixing simulations (D and E) of the binary solutions containing the complexes LCs^+Pic^- (0, 225, and 400 ps) LNa^+Pic^- (500 ps) with OPLS chloroform charges, and LCs^+Pic^- at 550 ps ("polar scaled OPLS" chloroform model). See Figure 1 for comments.

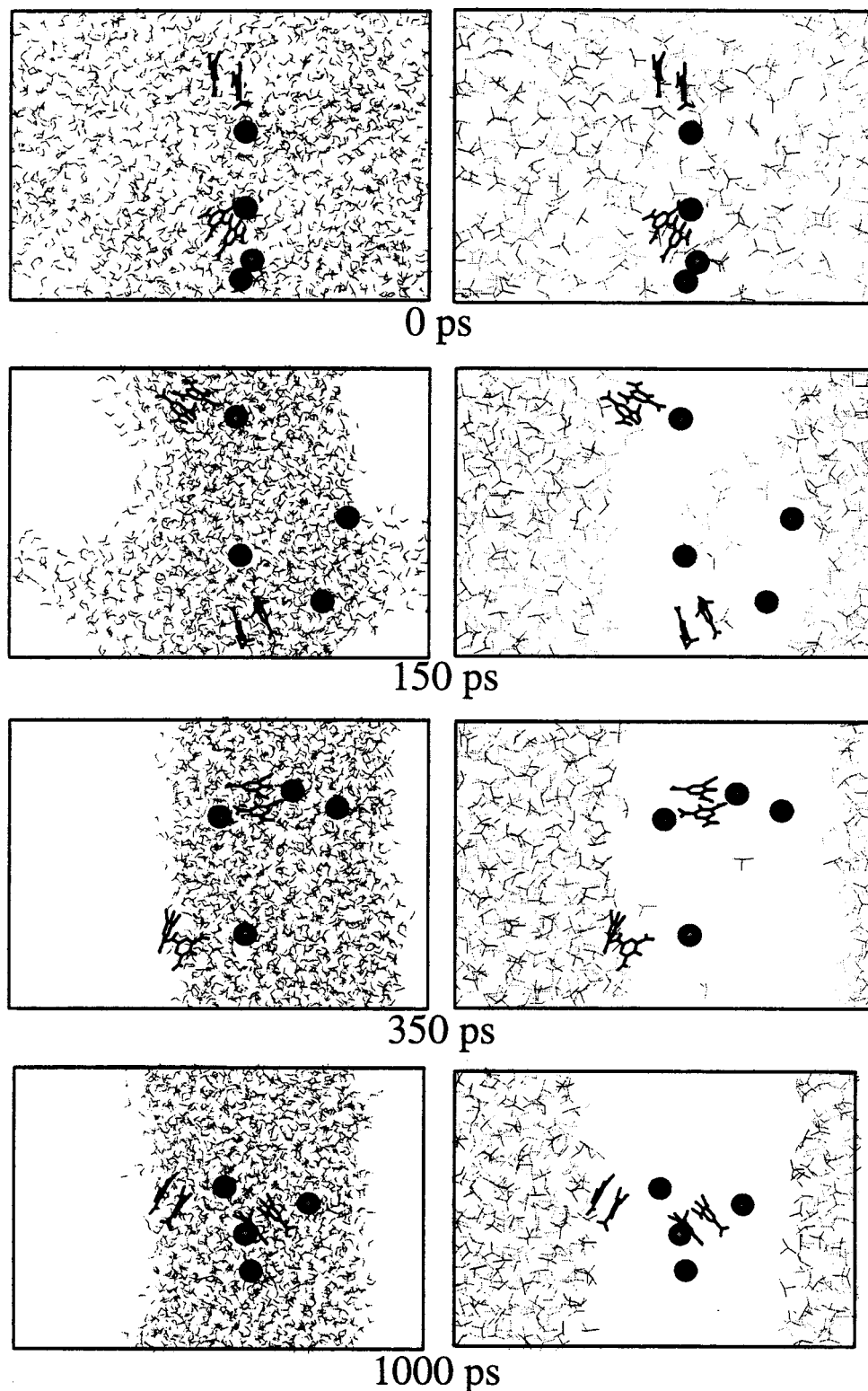


Figure 4. Demixing simulation (F) of the binary solution containing the $(\text{Cs}^+\text{Pic}^-)_4$ salt. See Figure 1 for comments.

side, while the Pic^- anion was “right at the border”. The final situation of LCs^+Pic^- was nearly identical to the one obtained from simulations which started from the two adjacent liquid phases,^{13,14} indicating that it indeed corresponds to a thermodynamic equilibrium.²³ The Pic^- anion displayed different relationships with the complex: it was separated from LCs^+ , but in loose contact with LNa^+ . The counterion and the reduced local concentration of water at the interface likely contributed to the stabilization of the (unstable) inclusive LNa^+ complex.

Both ions sit inside the crown ether moiety of **L**, but they are not fully shielded from water.

3. Demixing Simulations F – H: Binary Solutions of the $(\text{Cs}^+\text{Pic}^-)_4$ and $(\text{Cs}^+\text{NO}_3^-)_4$ Salts. For the $(\text{Cs}^+\text{Pic}^-)_4$ system, two simulations were performed, due to the fact that there was a question of possible stacking between Pic^- anions.²⁴ A first simulation of the $(\text{Cs}^+\text{Pic}^-)_4$ solution (F) started with the salts near the center of the solvent box, with two pairs of stacked Pic^- anions in contact with Cs^+ cation(s) (Figure 4). This

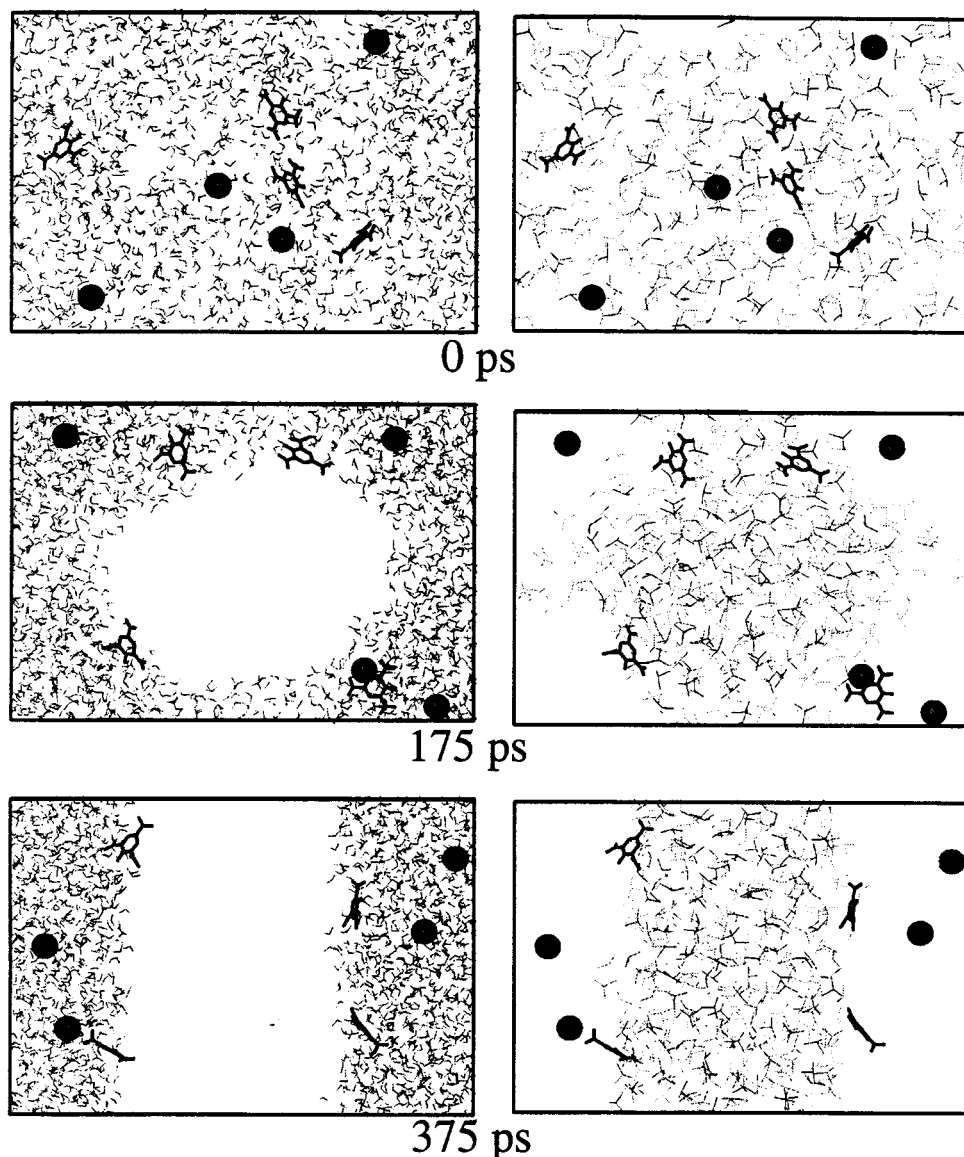


Figure 5. Demixing simulation (G) of the binary solution containing the $(\text{Cs}^+\text{Pic}^-)_4$ salt. See Figure 1 for comments.

mixture was obtained starting from a crystal fragment of the Pic^-Cs^+ salt,²⁵ immersed at the water–chloroform interface, and simulated at 500 K. Surprisingly, during the whole mixing stage (550 ps), two pairs of anions remained stacked despite their electrostatic repulsion. During the demixing process, the Cs^+ cations were progressively surrounded by water, while the two pairs of anions remained stacked. After 300 ps, one pair adsorbed finally at the interface, while the second one was immersed in water, surrounded by three to four cations, loosely coordinated to the oxygen atoms of Pic^- . This arrangement remained stable when the simulation was pushed up to 1 ns (Figure 4). As the dimers were surrounded by Cs^+ cations, we anticipated that the latter, which are hydrophilic, would prevent diffusion of the anions to the interface. This was indeed supported by a computer experiment which started with the configuration of this system after 1 ns and from which the Cs^+ cations were removed. As shown in Figure S3 (see Supporting Information), the $(\text{Pic}^-)_2$ dimer, which was in water, migrated to the interface where all anions spread.

This led us to develop another $(\text{Cs}^+\text{Pic}^-)_4$ system, where the ions were initially “randomly” diluted in the whole solvent system, without pairing. This was achieved by inverting the Cs^+ charge to -1 during the mixing stage at 500 K and running

550 ps of dynamics. The corresponding demixing simulation (G) shows, as in simulation F, that the cations were readily surrounded by water molecules, while a chloroform cluster formed gradually (see snapshot at 175 ps; Figure 5). All Pic^- anions were right at the border between water and chloroform. After 375 ps, the two phases were separated (Figure 5), leading to *two* interfaces, which are equivalent, due to the periodicity of the system.

Thus, simulations F and G do not converge to similar situations. It is important to point out that the $(\text{Cs}^+\text{Pic}^-)_4$ system simulated has a concentration of about 0.14 mol/L with respect to the aqueous phase, which is above the experimental solubility of this salt in water (about 10^{-3} mol/L²⁶). What really happens when salts are dissolved with a water–organic mixture is not known from experiment, and it is not clear which of the simulations F or G is most realistic. However, both simulations indicate that the Pic^- anions start forming a negatively charged “layer” at the interface, next to a diffused “layer” of positively charged Cs^+ cations. In addition, visual inspection of the trajectories reveal that the ions differ by their mobilities: the cations diffuse markedly in water, while the Pic^- anions are “immobilized” at the interface.

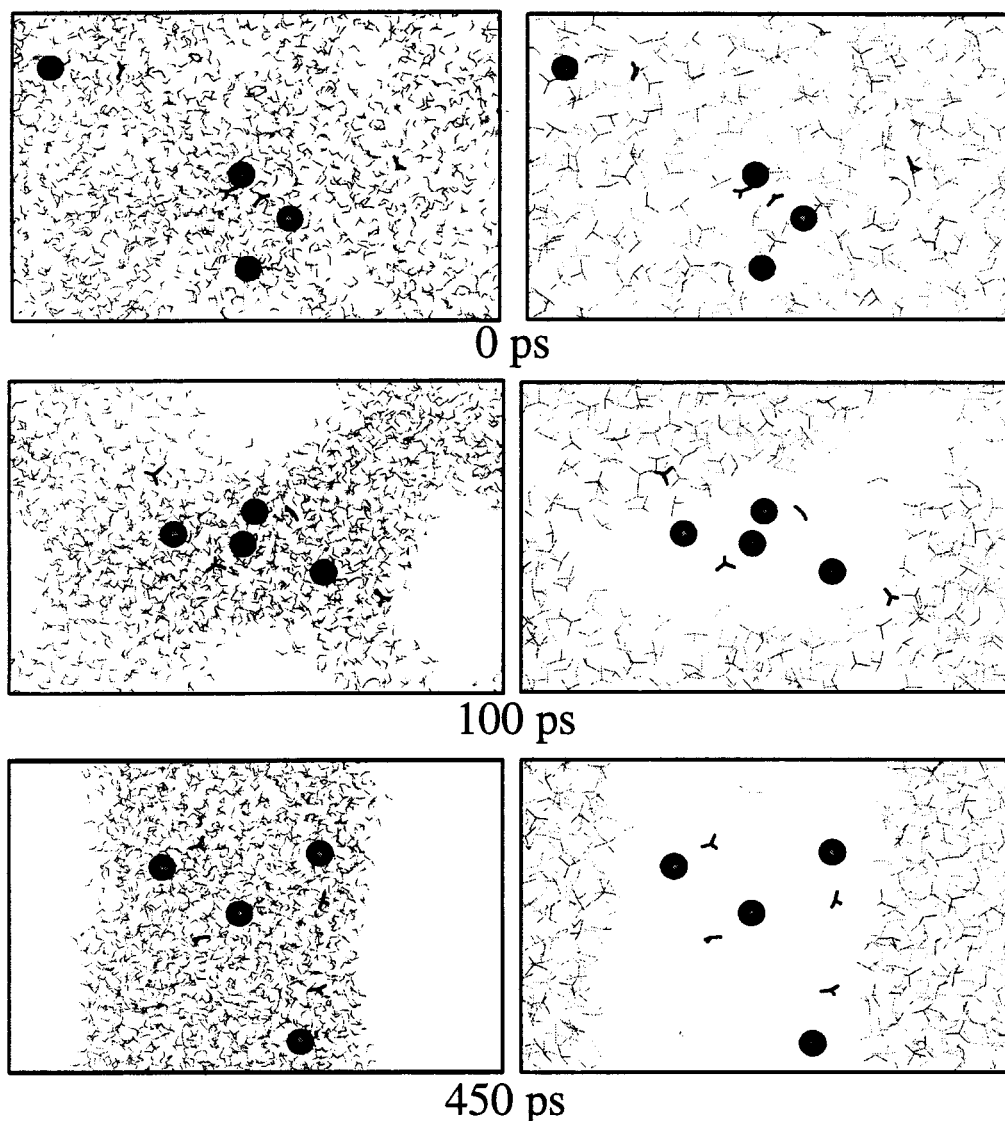


Figure 6. Demixing simulation (H) of the binary solution containing the $(\text{Cs}^+\text{NO}_3^-)_4$ salt. See Figure 1 for comments.

As far as liquid–liquid extraction is concerned, it can be speculated that, as the cations are extracted by the ionophores, their concentration in water decreases, which also facilitates the migration of Pic^- anions to the interface.

Solution of the $(\text{Cs}^+\text{NO}_3^-)_4$ Salt. For this simulation H, see Figure 6. Because the NO_3^- anion is more hydrophilic than Pic^- , the demixing of the $(\text{Cs}^+\text{NO}_3^-)_4$ solution led to a different situation, compared to the $(\text{Cs}^+\text{Pic}^-)_4$ solution. Indeed, after 400 ps, all NO_3^- and Cs^+ ions were completely immersed and diluted in the aqueous phase, oscillating at 7–12 Å from the interface.

4. Demixing Simulations I and J: Binary Solutions Containing Mixtures of the $(\text{Cs}^+\text{Pic}^-)_4$ and $(\text{Cs}^+\text{NO}_3^-)_4$ Salts, of L Uncomplexed, and of the LCs^+ Complex. In the above simulations, a single type of solute was considered. Next, we considered two more complex systems I and J. They contained a mixture of the $(\text{Cs}^+\text{NO}_3^-)_4$ and $(\text{Cs}^+\text{Pic}^-)_5$ salts, and three extractant molecules **L** (i.e., 9 Cs^+ , 5 Pic^- , 4 NO_3^- ions, and three **L** ligands). In mixture-1 (simulation I) **L** was uncomplexed, while in mixture-2 (simulation J), one **L** ligand complexed Cs^+ . The initial states (Figures 7 and 8) corresponded to “random” dilution of the solutes in the solvent box. In both cases, the Cs^+ and NO_3^- were rapidly immersed in water, while **L**, LCs^+ , and Pic^- species remained at the border region

between the two phases. Phase separation was found to be somewhat slower than with more diluted solutions which contained a single type of solute, because **L** and LCs^+ species diffused more slowly than the solvent molecules. In simulation J, LCs^+ displayed higher surface activity than **L**, as it adsorbed earlier at the interface than the two **L** ligands which remained for about 500 ps in the chloroform phase, together with a few water molecules (Figure 8). There is thus no strong driving force for diffusion of **L** from chloroform to the interface. At about 650 ps, the separation between the two liquids was complete, but the interfaces were not flat, even when the simulation J was pushed up to 1 ns: adsorption of **L** and LCs^+ led to water protuberances. **L** was anchored at about 6 Å from the interface either by its crown moiety, or by its lower rim, via a relay of hydrogen bonded water molecules (“water finger”²⁷). We notice that the latter situation is unfavorable for cation capture, while the first one would easily allow for cation capture via a least motion pathway. This orientation is also the one anticipated when the methoxy groups at the lower rim of **L** are replaced by more lipophilic chains.

In simulation I (no LCs^+ complex), no spontaneous complexation of Cs^+ by **L** was observed (Figure 7). We noticed again the stabilization of a $(\text{Pic}^-)_2$ dimer in water and the high surface activity of Pic^- anions which attracted some Cs^+ cations

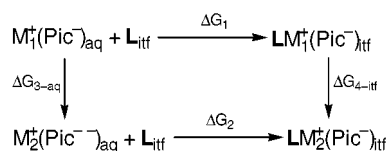
TABLE 2: Free Energy Calculations on the LM⁺ Complexes at the Interface and M⁺ in Water (kcal/mol)

calculations ^a	time ^b		Na ⁺ → K ⁺	K ⁺ → Rb ⁺	Rb ⁺ → Cs ⁺	K ⁺ → Cs ⁺	Na ⁺ → Cs ⁺
Na ⁺ /Cs ⁺	3 × 11 × (2 + 3) = 165	ΔG_{3-aq}	17.6	5.1	7.7	12.8	30.4
LNa ⁺ /LCs ⁺	1 × 51 × (2 + 3) = 255	ΔG_{4-itf}					23.7
		$\Delta\Delta G$					6.7
LCs ⁺ /LNa ⁺	3 × 21 × (4 + 6) = 630	ΔG_{4-itf}	11.8	3.9	6.3	10.2	22.0
		$\Delta\Delta G$	5.6	1.2	1.4	2.8	8.4
LK ⁺ /LNa ⁺	21 × (4 + 16) = 420	ΔG_{4-itf}	16.1	(3.9) ^c	(6.3) ^c	(10.2) ^c	26.3
		$\Delta\Delta G$	1.5	(1.2) ^c	(1.4) ^c	(2.8) ^c	4.1
LCs ⁺ Pic ⁻ /LNa ⁺ Pic ⁻	1 × 51 × (2 + 3) = 255	ΔG_{4-itf}					14.8
		$\Delta\Delta G$					15.6
LNa ⁺ Pic ⁻ /LCs ⁺ Pic ⁻	1 × 51 × (2 + 3) = 255	ΔG_{4-itf}					17.3
		$\Delta\Delta G$					13.1
LNa ⁺ Pic ⁻ /LCs ⁺ Pic ⁻	3 × 21 × (2 + 3) = 315	ΔG_{4-itf}	6.4	3.9	6.6	10.5	16.9
		$\Delta\Delta G$	11.2	1.2	1.1	2.3	13.5
LCs ⁺ Pic ⁻ /LNa ⁺ Pic ⁻	3 × 21 × (4 + 6) = 630	ΔG_{4-itf}	5.5	4.1	6.0	10.1	15.6
		$\Delta\Delta G$	12.1	1.0	1.7	2.7	14.8
LK ⁺ Pic ⁻ /LNa ⁺ Pic ⁻	21 × (4 + 16) = 420	ΔG_{4-itf}	5.4	(4.1) ^c	(6.0) ^c	(10.1) ^c	15.5
		$\Delta\Delta G$	12.2	(1.0) ^c	(1.7) ^c	(2.7) ^c	14.9

^a Initial/final state of the mutation. For consistency, the ΔG 's are given from the small to the large cation. ^b Total simulated time for the mutation = number of runs × number of windows × (picoseconds of equilibration + picoseconds of data collection). ^c The values reported for K⁺ → Rb⁺ and Rb⁺ → Cs⁺ correspond to mutations of 210 ps.

a few angstroms from the interface. Figures 7 and 8 also make clear that the concentrations of **L** or LCs⁺ were too low to form a monolayer.

5. Ion Recognition at the Interface. Because both LNa⁺ and LCs⁺ complexes adsorb at the interface, it was important to investigate which of these complexes is the most stable, in relation to the Cs⁺ extraction selectivity observed experimentally. For this purpose, we defined a thermodynamic cycle



where the free M⁺ cations sit in water (as shown by the above simulations) and their LM⁺ complexes sit at the interface “itf”. According to this cycle, the ion recognition at the interface, defined by $\Delta\Delta G = \Delta G_1 - \Delta G_2$, is equal to $\Delta G_{3-aq} - \Delta G_{4-itf}$, obtained by the “alchemical route”.^{28,29} The results are reported in Table 2. We calculated ΔG_{4-itf} first with a Pic⁻ counterion close to LM⁺ at the interface and then without counterion. The LCs⁺/LNa⁺ mutations were performed in both ways, starting respectively with LNa⁺ and with LCs⁺ first in a single run of 51 windows of 2 + 3 ps each. Two other series of LNa⁺/LCs⁺ mutations were repeated via explicit Rb⁺, K⁺ ions as intermediates (using 21 windows at each step and running additional 30 ps of equilibration at each cation). The sampling at each window was respectively 2 + 3 ps and 4 + 6 ps. In the presence of Pic⁻ counterion, the three procedures gave similar average values of ΔG_{4-itf} (16.0 ± 2.0, 16.9 ± 0.2, and 15.6 ± 0.2 kcal/mol, respectively, for Na⁺/Cs⁺ complexes), indicating that the smallest cation interacts best with **L**. In the absence of counterion, ΔG_{4-itf} was still larger (between 22.0 and 23.7 kcal/mol). For the K⁺/Cs⁺ complexes, however, all values of ΔG_{4-itf} are nearly identical, be the counterion present or not. There is thus no counterion effect on the K⁺/Cs⁺ binding by **L**, as these cations display a similar binding mode to the ligand (near the center of the crown ether moiety), and the Pic⁻ counterion is similarly adsorbed at the interface, loosely interacting with the complex (Figure 9). In the case of the LNa⁺ complex, the binding mode may somewhat differ, because Na⁺, too small for the crown of **L**, may fluctuate between “endo” binding (close to the phenoxy oxygens) and “exo” binding, both possibly

involving co-complexation of one water molecule.³⁰ This is why the ΔG_{4-itf} energies corresponding to the LNa⁺/LK⁺ mutations are more sensitive to the sampling conditions and to the presence of counterions. With 21 windows of 4 + 6 ps, we obtain a ΔG_{4-itf} of 11.8 kcal/mol (no counterion) and of 5.5 kcal/mol (with Pic⁻ counterion). Repeating these mutations with 21 windows of 4 + 16 ps (i.e., in 420 ps) leads to 16.1 and 5.4 ± 0.2 kcal/mol, respectively. Thus, all simulations on LM⁺Pic⁻ complexes give similar ΔG_{4-itf} values, while for the LNa⁺/LK⁺ complexes (no counterion), ΔG_{4-itf} is still increased with the largest sampling. We notice that in the latter case, the Na⁺ cation sits “exo”, cocomplexed with one H₂O molecule hydrogen bonded to two phenoxy oxygen atoms. In the LNa⁺Pic⁻ complex, no such cocomplexation of water is observed, and the cation sits closer to the center of the crown ether, presumably attracted by the Pic⁻ counterion which stacks over a phenoxy ring (Figure 9). Thus, in all cases, Na⁺ interacts best with **L** at the interface.

However, taking into account the difference in dehydration energies ΔG_{3-aq} of the ions leads to positive values of $\Delta\Delta G$ (i.e., to the *selective binding of Cs⁺ at the interface* (Table 2)). The calculated order of binding affinities at the interface (Na⁺ < K⁺ < Rb⁺ < Cs⁺) is the same as the experimental order of free energies of extraction by **L** from water to chloroform.^{5,7} At a quantitative level, the numbers cannot be simply compared, because **L** is conformationally mobile and extracts Cs⁺ in the 1,3-alternate conformation but extracts (weakly) Na⁺ in the cone conformation. In our simulations, **L** remains 1,3-alternate in all cation complexes, such as in the conformationally locked 1,3-dialkoxy analogues of **L**, which also display the same order of extraction selectivities.⁷ Concerning the K⁺/Cs⁺ binding by **L**, we notice that the $\Delta\Delta G$'s calculated at the interface in the absence or in the presence of the Pic⁻ anion (2.8 and 2.7 ± 0.2 kcal/mol, respectively) are remarkably close to the differences in binding free energies obtained in water saturated chloroform solution for the 1,3-alternate 1,3-diisopropoxy analogue of **L** (3.0 kcal/mol).⁷ For the Na⁺/K⁺ ions, the difference is larger and calculated to be anion dependent. A more quantitative assessment of the Na⁺/K⁺ binding may require time scales larger than 420 ps and a more elaborate representation of the potential energy, involving polarization and many-body effects.^{31,32} We compared in ref 13 different electrostatic representations of **L** and found that the binding sequence in water was the same with

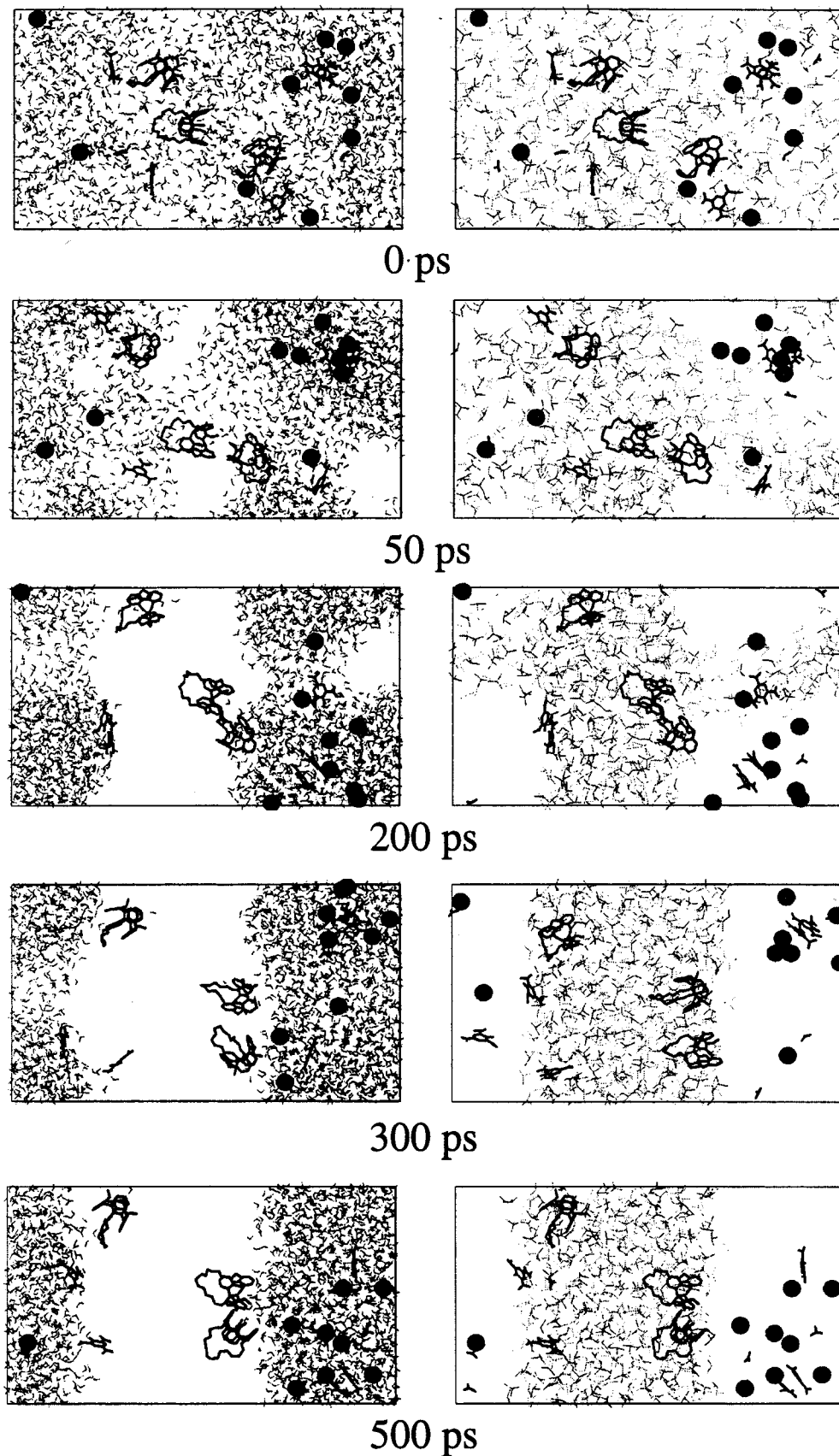


Figure 7. Demixing simulation (I) of the binary solution containing the “mixture-1”: $(\text{Cs}^+\text{NO}_3^-)_4$, $(\text{Cs}^+\text{Pic}^-)_5$, 3 L. See Figure 1 for comments.

several sets of charges. Concerning the physical representation of the system, it should also be pointed out that other effects (e.g., saturation of the interface by free or complexed ligands

or by lipophilic ions) which modify the local environment of the complex, may also modify the relative free energies of binding at the interface.

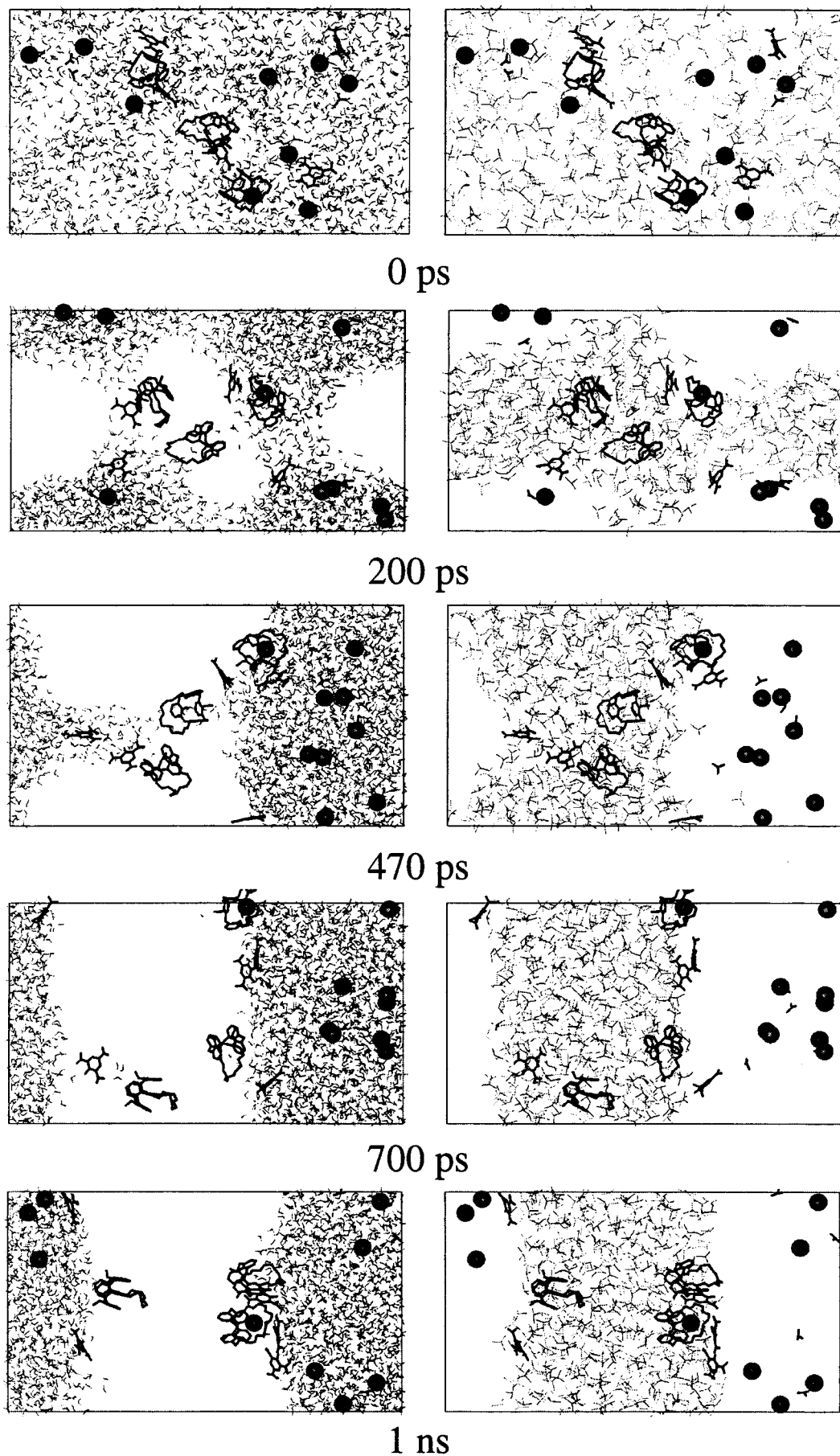


Figure 8. Demixing simulation (J) of the binary solution containing the “mixture-2”: $(\text{Cs}^+\text{NO}_3^-)_4$, $(\text{Cs}^+\text{Pic}^-)_4$, 2 **L** and **LCs**⁺ **Pic**[−]. See Figure 1 for comments.

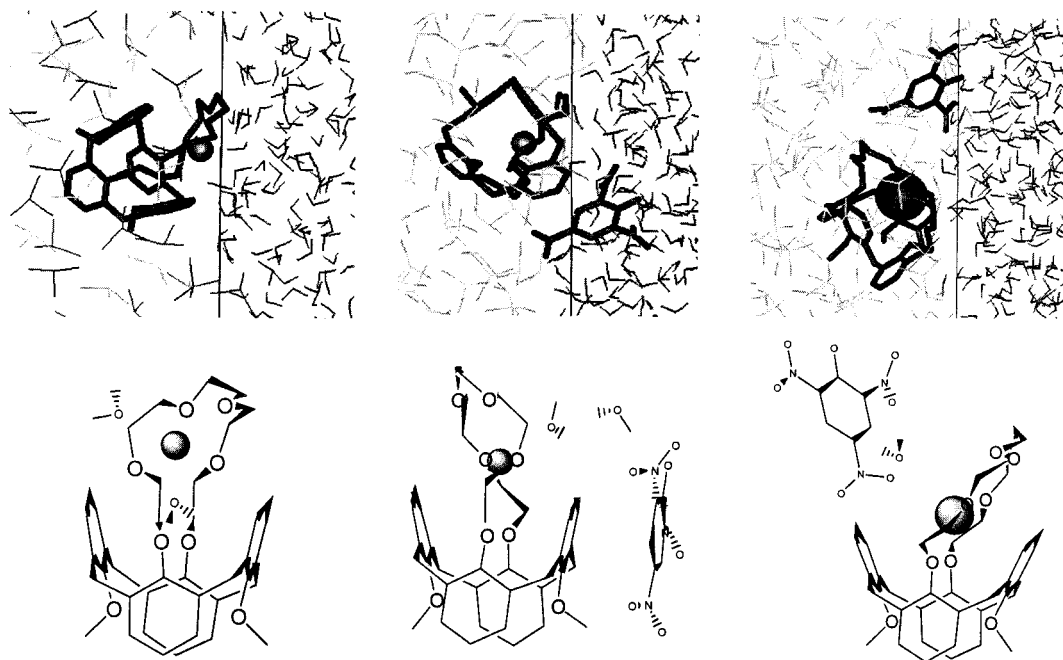


Figure 9. The LNa^+ , $\text{LNa}^+ \text{Pic}^-$, and $\text{LCs}^+ \text{Pic}^-$ complexes (from left to right) at the water–chloroform interface (top). Bottom: the complexes are reoriented to highlight the binding mode of the cation.

IV. Discussion and Conclusion

There have been a number of computer simulations (Monte Carlo or MD) on binary solutions involving liquids of low miscibility (Lennard-Jones particles^{33–37} or molecules,^{38,39} oil–water mixtures^{40,41} or hydrophobic mixtures such as water–methane/methanol⁴² or water–decanol⁴³). Here we report the first simulations on the phase separation of binary solvent mixtures containing ionic species and complexes which are involved in the assisted ion transfer from the aqueous to the organic phase. The results provide valuable insights into microscopic events that take place during the primary stages of ion recognition and extraction. In all cases, demixing leads to two liquid phases separated by a narrow interface, but the outcome depends on the nature of the solute. We will first discuss the rates and driving forces for phase separation. Then, based on the computational results, we propose a mechanism for assisted ion extraction and recognition.

1. Rate of Demixing. Although all systems demix quite readily, one can wonder to what extent the rate of “microscopic demixing” depends on the nature and concentration of the solution. Indeed, it is generally considered that addition of salts or surfactants increases the rate of demixing. For this purpose, we followed the demixing index χ_{demix} , calculated as described in the method section. Figure 10, where χ_{demix} is plotted as a function of time for most of them. χ_{demix} decreases exponentially from about 0.9 (mixed state) to 0.2 (separated phases). The final value is not exactly zero because the densities of the liquids overlap in the interfacial region. We fitted an exponential model to χ_{demix} of the following type: $\chi_{\text{demix}} = (\chi_0 - \chi_\infty)\exp(-K_s t) + \chi_\infty$. The values of the parameters are reported in Table 3. The initial demixing rate, given by the $(\chi_0 - \chi_\infty)K_s$ product, as well as the K_s values indicate that the demixing is somewhat slower with the mixture of solutes (J), and faster with $\text{LCs}^+ \text{Pic}^-$ (D) and $(\text{Cs}^+ \text{Pic}^-)_4$ (G), than in the neat binary solution (A). The differences are small and not simple to interpret in terms of the hydrophilic/amphiphilic nature and concentration of the solutes. Additional simulations are required to elucidate the role of the

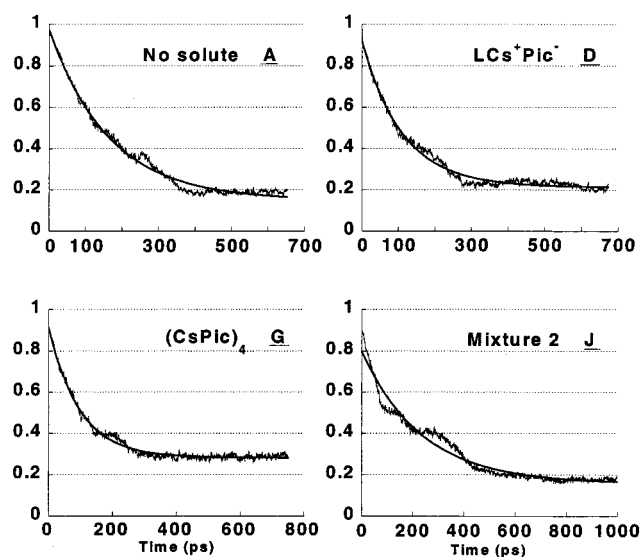


Figure 10. “Demixing rate” of selected systems. The χ_{demix} index is plotted as a function of time (picoseconds).

TABLE 3: Parameters of the χ_{demix} Curves of Figure 9

solute	no solute A	$\text{LCs}^+ \text{Pic}^-$ D	$(\text{Cs}^+ \text{Pic}^-)_4$ G	mixture 2 J
$K_s (\pm 5 \times 10^{-5})$	0.0061	8.9×10^{-3}	10.3×10^{-3}	4.2×10^{-3}
$\chi_0 (\pm 0.003)$	0.973	0.915	0.916	0.799
$\chi_\infty (\pm 0.001)$	0.150	0.214	0.283	0.157
initial rate ($\pm 0.3 \times 10^{-3}$)	4.5×10^{-3}	6.3×10^{-3}	6.5×10^{-3}	2.7×10^{-3}

concentration of the solutes and shape of the simulation box. On the experimental side there are, to our knowledge, neither data concerning these systems nor kinetic data of phase separation at the time scales simulated. According to the phase separation experiments, once droplets are formed in a given phase, gravitational and viscosity effects, negligible at the microscopic level, become dominant. The volume and precise shape of the container also determine the rate of macroscopic phase separation.

TABLE 4: Energy Component Analysis (kcal/mol) at the Beginning (10–60 ps) and at the End (last 50 ps) of the Demixing Simulations of Selected Solutions. \pm Corresponds to the Fluctuations

solute	LCs ⁺ Pic ⁻ (D)			mixture 2 ^a I		
	begin	end	ΔE	begin	end	ΔE
L/Cs ⁺	-48 \pm 3	-54 \pm 3	-6	-45 \pm 11	-43 \pm 6	2
L/Chl.	-41 \pm 5	-48 \pm 4	-7	-87 \pm 6	-155 \pm 6	-68
L/Wat.	-16 \pm 5	-4 \pm 3	1	-144 \pm 10	-50 \pm 7	94
Cs ⁺ /X ⁻	-41 \pm 4	0 \pm 0	41	-611 \pm 20	-654 \pm 30	-43
Cs ⁺ /Chl.	-5 \pm 3	-5 \pm 2	0	3 \pm 8	0 \pm 4	3
Cs ⁺ /Wat.	-39 \pm 7	-39 \pm 7	0	-780 \pm 39	-837 \pm 44	-57
X ⁻ /Chl.	-17 \pm 4	-18 \pm 4	-1	-86 \pm 8	-102 \pm 5	-16
X ⁻ /Wat.	-84 \pm 9	-92 \pm 8	-8	-677 \pm 25	-703 \pm 33	-26
Wat./Chl.	-1494 \pm 156	-389 \pm 16	1105	-1671 \pm 207	-298 \pm 16	1373
Wat./Wat.	-13500 \pm 158	-14537 \pm 42	-1037	-15000 \pm 184	-15830 \pm 62	-830
Chl./Chl.	-1641 \pm 94	-2359 \pm 17	-718	-2019 \pm 147	-3141 \pm 22	-1122
total	-16789 \pm 104	-17413 \pm 38	-624	-20538 \pm 120	-21092 \pm 83	-554

solute	(Cs ⁺ Pic ⁻) ₄ G			no solute A		
	begin	end	ΔE	begin	end	ΔE
4Cs ⁺ /4X ⁻	-111 \pm 10	-170 \pm 15	-59			
4Cs ⁺ /Chl.	1 \pm 5	-0 \pm 4	-1			
4Cs ⁺ /Wat.	-432 \pm 21	-427 \pm 18	5			
4X ⁻ /Chl.	-85 \pm 11	-94 \pm 10	-9			
4X ⁻ /Wat.	-330 \pm 26	-294 \pm 18	36			
Wat./Chl.	-1346 \pm 188	-349 \pm 13	997	-1655 \pm 172	-292 \pm 15	1363
Wat./Wat.	-12977 \pm 225	-13828 \pm 58	-851	-14221 \pm 173	-15416 \pm 46	-1195
Chl./Chl.	-1540 \pm 109	-2228 \pm 15	-688	-1629 \pm 114	-2549 \pm 17	-920
total	-16680 \pm 128	-17232 \pm 56	-552	-17505 \pm 116	-18257 \pm 46	-752

^a For this system, the values reported for **L** correspond to the total for the three ligands, those for Cs⁺ correspond to the nine cations, and those for X⁻ correspond to the five Pic⁻ + the four NO₃⁻ anions.

2. Solvent–Solvent Interactions as Driving Forces for Phase Separation. The thermodynamics of solvent–solvent separation involves enthalpic and entropic components, which cannot be simply assessed from the simulations. We decided, however, to compare the interaction energies between different groups of the systems at the beginning (first 10–60 ps) and at the end (last 50 ps) of the demixing simulations to elucidate which of the interactions become attractive or repulsive upon phase separation. For this purpose, the solute was split into its **L**, Cs⁺, and X⁻ components. The results obtained for selected systems (Table 4) show that, upon demixing, the total interaction energies become more attractive by about 500 to 750 kcal/mol. The energy changes which involve the solutes (cation/anion, or ion–water interactions) are small (about 50 kcal/mol or less) compared to those involving the solvent–solvent interactions (about 1000–1400 for water–chloroform, -830 to -1200 for water–water and -700 to -900 kcal/mol for chloroform–chloroform). The gain in water–water interactions is smallest with the concentrated salt (Cs⁺Pic⁻)₄ and largest for the pure liquid mixture. These numbers thus suggest that *phase separation is driven by the cohesive forces of the solvents, and mostly water*, which has the highest surface tension and tends to self-aggregate. This conclusion is consistent with the above observation that the demixing times and rates are comparable for all simulated systems. The formation of a flat, instead of spherical interface between water and chloroform results from the minimization of the interfacial area, when the system is simulated with periodic boundary conditions.

3. Where Are the Ions and the Complexes after Separation of the Liquids? Implications for the Extraction Mechanism. The solutes are found in different locations after separation of the two liquid components, depending on their hydrophilic–hydrophobic character. It is important to notice that, at the end, none of the species is fully immersed in the organic phase. In particular the ligand **L** and its LM⁺ complexes, known to be extracted and more soluble in the organic than in the aqueous

phase, adsorb instead at the interface like surfactants: their hydrophobic groups sit on the organic side and the hydrophilic ones (cation and crown ether) are anchored at the interfacial water molecules, via attractive interactions.²³ As expected, the uncomplexed hydrophilic Cs⁺ cations are fully immersed in the aqueous phase.

Concerning the anions, different situations are found, depending on their hydrophilicity and on whether the cation is complexed. For instance, Cl⁻, although hydrophilic, finally forms in two simulations an intimate pair with the LCs⁺ complex and therefore sits very close to the interface. Other simulations lead to Cl⁻ capture by water, leading to a positively charged interface. Which of the two situations is most stable is unclear, as they seem separated by some energy barrier due to the solvent reorganization. At the early stages of the demixing process, however, the local water concentration may be in some cases low enough to facilitate Cl⁻ pairing with LCs⁺. In the case of uncomplexed Cs⁺NO₃⁻ salt, both ions are fully solubilized in water, while the Pic⁻ anions display a remarkable interface activity, be the accompanying cation free (Cs⁺Pic⁻ solution) or complexed (LCs⁺Pic⁻ or LNa⁺Pic⁻ solutions). Such amphiphilic behavior of anions is important for the mechanism of assisted ion extraction (see next section), as well as for the electrical properties of the interface.⁴⁴

The distribution of ions obtained after demixing follows the same trends as those simulated for more concentrated solutions of M⁺X⁻ salts (K⁺Cl⁻, K⁺ClO₄⁻, K⁺Pic⁻, NMe₄⁺ Cl⁻, guanidinium⁺Cl⁻, nonyltrimethylammonium⁺Cl⁻).⁴⁸ It is noteworthy that ions, such as ClO₄⁻, Pic⁻, BPh₄⁻, dicarbolides, AsBPh₄⁺, NMe₄⁺, and guanidinium⁺, are surface active, although they do not possess, like classical surfactants, a polar head flanked by a lipophilic tail.⁴⁸ Another feature of interest concerns the tendency of like-charged ion pairs such as guanidinium⁺...guanidinium⁺ or Pic⁻...Pic⁻ to display stacking arrangements in pure water solution where the ions “attract each other”.^{24,48}

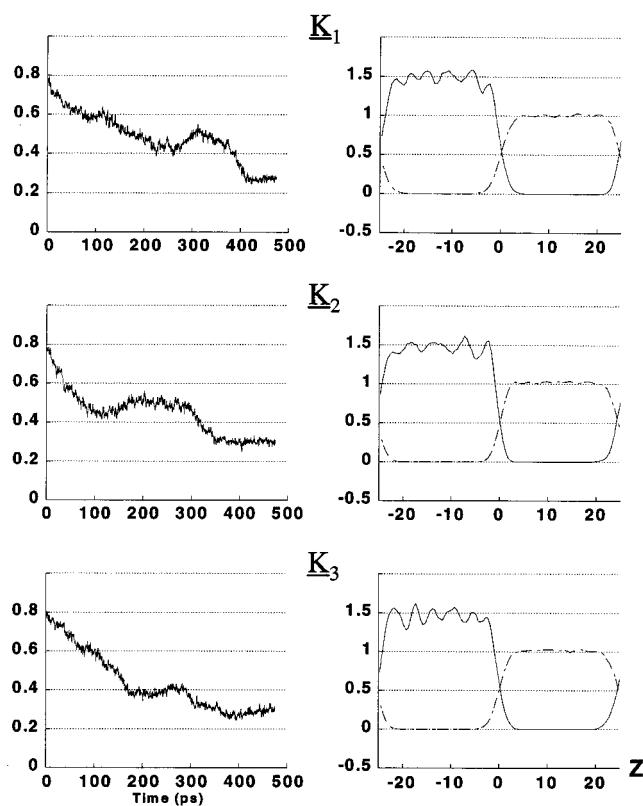


Figure 11. Demixing simulation (K) of the binary water–chloroform solution (no solute). Simulations performed with three models of chloroform: (a) OPLS model (K_1), (b) all atom model without polarization (K_2), (c) all atom from ref 20 with polarization (K_3). Left: demixing index χ_{demix} . Right: density profiles after phase separation.

4. Suggested Mechanism of Assisted Ion Extraction. From a mechanistic point of view, our results suggest that *cation uptake and recognition by the ionophore take place at the interface* between droplets of “oil” and water. The high rate of microscopic phase separation suggests that, even in the hypothetical starting situation of perfectly mixed solutions, *droplets form on the nanosecond time scale*. Cation capture is thus very unlikely to occur in an homogeneous mixed solution. Our simulations show that from the early stages until the end of microscopic phase separation, the free ionophore sits at the border between the aqueous and organic liquids. In more concentrated conditions, ionophores should concentrate at the interface, forming assemblies which may range from a monolayer to more or less concentrated aggregates.^{45–48} Lipophilic anions also accumulate at the interface, where they attract cations^{48,49} which would be otherwise “repelled” by the interface.⁵⁰ This is likely an important feature of synergistic

effects displayed by some anions, as well as by co-extractant molecules that accumulate in the interfacial region.

An important feature of the interfacial region is the reduced water content, which favors complexation, such as in an apolar environment. Once a complex is formed, there comes the question of why it diffuses to the organic phase. Indeed, we find that the complex is also highly surface active, and even more active than the free ionophore, due to its enhanced amphiphilic character. We suggest that *its departure from the interface to the organic phase is facilitated by the saturation of the interface* (which reduces the surface tension) and likely driven by the concentration of ions and ionophores, as well as by the presence of other species (“salting out” effects due to the high salt content of the source aqueous phase, as well as synergistic effects due to cocomplexant and surface active anions or ligands). This mechanism is consistent with kinetic models of related systems,^{1,3} and with the experimental observation of monolayers of extractant molecules such as calixarenes,⁵¹ valinomycin,⁵² TBP,⁵³ crown ethers,⁵⁴ and phosphoric acid derivatives⁵⁵ at the air–water interface where they may capture ions from the aqueous phase (see below).

Another important feature concerns the question of *ion discrimination at the interface*. Our FEP calculations reveal a clear preference for Cs^+ over Na^+ uptake by **L**, which is the same as the selectivity observed in extraction or transport experiments by the conformationally mobile **L** ligand, as well as by its 1,3-alternate conformationally locked analogues. This is fully consistent with the results of Kunitake et al.⁵¹ and Baglioni et al.^{56–59} on the selective complexation of cations by calixarenes in monolayers at the air–water interface.

Concerning the high Cs^+ affinity and Cs^+/Na^+ selectivity of **L** and of related 1,3-alternate derivatives, compared to extractant like crown ethers, several features are noticed. First, the uncomplexed calixarene ligands are more amphiphilic and surface active than the crown ethers. Second, in the crown ether complexes, the cation is much less shielded from the solvent than in the calixarene complexes, where the cation also enjoys “cation- π ” interactions. The water environment destabilizes the crown ether complexes more than the calixarene ones. Indeed, according to MD simulations on $(18\text{-crown-6} \cdot \text{K}^+ \text{Pic}^-)_6$ at the liquid–liquid interface, some K^+ cations decomplex,⁴⁵ whereas all complexes of a $(\text{LCs}^+ \text{Pic}^-)_9$ aggregate remain of inclusive type.⁴⁸ In another study, we showed that traces of water in a “humid chloroform” solution lead to a $\text{LCs}^+/\text{LNa}^+$ selectivity closer to the one in pure water than in dry chloroform.⁶⁰ Thus, more generally, when hydration forces are dominant, *the selectivity found at the water–chloroform interface should also operate at other aqueous interfaces such as micelles, water–membrane interfaces*.

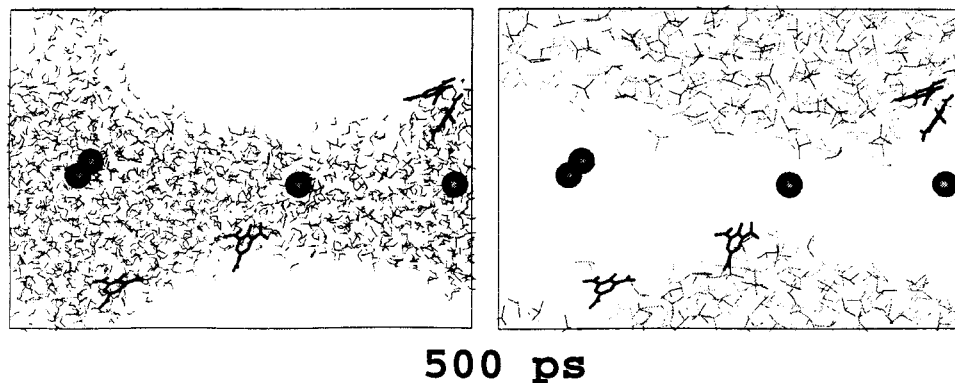


Figure 12. Demixing simulation of the binary solution containing the $(\text{Cs}^+ \text{Pic}^-)_4$ salt. Calculation with Ewald. See Figure 1 for comments.

5. Computational Aspects. The computations reported here are exploratory and, like most of the related computations on ions and molecular species at interfaces^{27,61–63} or on mixed liquid systems^{43,64–69} make a number of approximations. Concerning the energy representation of the system, an important feature concerns the mutual interactions between water and the organic solvent. They were calculated using a 1–6–12 Lennard-Jones potentials fitted for the pure liquid phases, and using standard combination rules for van der Waals interactions between unlike atoms. In principle, it would be desirable to account explicitly for polarization effects.^{20,70,71} The TIP3P water model, which implicitly includes some self-polarization energy, may be too polar to depict interactions with chloroform. Conversely, the polarization of chloroform molecules by water is not accounted for in the OPLS model. As pointed out in ref 72, the dielectric properties of water near the surface may differ considerably from those in the bulk. The hydrogen bonding capacity of water is enhanced by polarization effects.⁷³ We therefore wondered as to what extent the fast demixing observed in the MD simulations and the nonextraction of the LCs^+ complex might be an artifact resulting from an underestimation of the water–chloroform interactions.

This led us to undertake additional simulations with more polar representations of chloroform. Following a procedure adopted by Kovacs et al.,⁷⁴ we first simulated another demixing of the LCs^+Pic^- solution (same system as in simulation D) where the OPLS chloroform charges were scaled by 1.3, to enhance its electrostatic interactions with water and the solutes. With this more polar model, separation of the two liquids also took place, although somewhat more slowly (in about 550, instead of 400 ps), also leading to adsorption of LCs^+ and the Pic^- anion at the interface (Figure 3). LCs^+ was somewhat deeper in the organic phase than in the simulation with OPLS charges, but also remained in contact with water. In the two simulations, however, the organic phase remained dry. This is consistent with the low solubility of water in chloroform (about 0.1% in weight^{75,76}), according to which the chloroform slab should contain at most one water molecule.

Another series of simulations K considered the neat water–chloroform system, where chloroform was represented with three models: the OPLS model (K_1) and the all atom model of Chang et al.²⁰ used without polarization (K_2) and with polarization²⁰ (K_3). The cutoff distance was also larger (13.5 Å) than that in the standard calculations (12 Å). Because the calculations with polarization are quite computer demanding, all simulations K were performed on a system smaller than in A (Table 1). The demixing index χ_{demix} plotted as a function of time and the density curves obtained from the simulations (Figure 11) reveal a very similar behavior with all three models (see also snapshots in Figure S4 (Supporting Information)). Demixing was completed in less than 450 ps, leading to nearly identical interfacial widths, solvent densities, and anhydrous organic phases. These results validate those reported above with the OPLS model. When compared to those obtained with a larger box (simulation A), they also reveal no marked effect of the size of the solvent system. We noticed that demixing K_2 or K_3 were somewhat less smooth than demixing A (see χ_{demix} in Figures 10 and in 11), and that they do not all follow the same “path” (Figure S4). Thus, the detailed pathway for phase separation may depend on the size and shape of the simulation box, in conjunction with the treatment of boundary conditions.

The treatment of long-range electrostatic interactions may also determine the dynamics and calculated properties of the system.^{77,78} To gain some insight into this effect, we decided

to simulate the demixing of the $(\text{Cs}^+\text{Pic}^-)_4$ solution (same starting state as in simulation G), using the particle mesh Ewald summation technique.²¹ As these simulations are more time-consuming than those without Ewald, they were performed for 500 ps only. With Ewald, demixing was slower than without Ewald and not completed after 500 ps. At the end of the simulation, the two liquid phases were almost completely separated, but the interface was not flat. However, the environment of the ions looks very much like the one obtained without Ewald: the Cs^+ cations are immersed in the aqueous phase, while the Pic^- anions sit at the border between the two liquid phases (Figure 12). This comparison thus suggests that long range electrostatic forces do not critically determine the outcome of the demixing process. It is also important to remember that the Ewald method that was used assumes a three-dimensional periodic representation of the system, which is obviously not the case. On the other hand, the two-dimensional version of Ewald, which is more appropriate for planar interfaces,⁷⁹ is expected to favor the demixed, relative to the mixed state of the solution.

In addition to these methodological questions, the physical representation of the system is of importance. *Increasing the concentration of the solutes modifies their interfacial properties.* For instance, when simulated at the interface, the $(18\text{-crown-6}\cdot\text{K}^+\text{Pic}^-)_1$ complex remained adsorbed for 1 ns, while the $(18\text{-crown-6}\cdot\text{K}^+\text{Pic}^-)_6$ system displayed rapidly an equilibrium where some cations decomplexed, others remained complexed at the interface, and another was extracted to the organic phase.⁴⁵ This contrasts with the simulation of the $(\text{LCs}^+\text{Pic}^-)_9$ “layer” system at the interface where all complexes remained of inclusive type, presumably due to the better cation shielding from the solvent, and the larger host–guest interactions with L .⁴⁸ The comparison of monovalent to di- or trivalent ions also reveals interesting differences in interfacial behavior, which likely corresponds to differences in demixing processes.^{48,80} There is thus an intimate relationship between the demixing process of the binary water–organic solutions and the interfacial behavior of ionic^{27,61}–neutral⁸¹ solutes. As pointed out in ref 48, the surface of water and liquid–liquid interfaces are peculiar key borders and meeting areas where extractant molecules and ions concentrate, leading to supramolecular organization, recognition, and subsequent processes. Thus, computer simulations are becoming of increasing importance to provide dynamic microscopic pictures of interfaces, whose status may range from stimulating mental pictures to representations of a “complex reality”. Beyond simple phase separation and solubilization of the ions or their complexes, computer simulations contribute to our understanding of related complex phenomena like formation of third phases, or of self-assembled organized structures such as micelles or mesophases,^{82–86} layers of amphiphilic surfactant molecules,^{87–89} and membranes.^{67,90,91}

Acknowledgment. The authors are grateful to CNRS IDRIS and Université Louis Pasteur for allocation of computer time, to PRACTIS and EEC (F14WCT96-0022) for support, and to S. Seethaler for linguistic assistance.

Supporting Information Available: Figures of the demixing simulations Band C' of the LCs^+Cl^- complexes, the demixing simulation F of the $(\text{Cs}^+\text{Pic}^-)_4$ salt, and the demixing simulations K_1 – K_3 of the binary water–chloroform solutions (4 pages). Ordering information is given on any current masthead page.

References and Notes

- (1) Moyer, B. A. Basic principles of extraction and liquid-liquid systems employing crown ethers and related metal-ion receptors. In *Comprehensive*

Supramolecular Chemistry. Molecular Recognition: Receptors for Cationic Guests; 1996, Atwood, J. L., Davies, J. E. D., McNicol, D. D., Vögtle, F., Lehn, J.-M., Eds.; Pergamon: Elmsford, NY, 1996; pp 325–365.

(2) Koenig, K. E.; Lein, G. M.; Stuckler, P.; Kaneda, T.; Cram, D. J. *J. Am. Chem. Soc.* **1979**, *101*, 3553.

(3) Danesi, P. R. Solvent extraction kinetics. In *Principles and Practices of Solvent Extraction*; Rydberg, J., Musikas, C., Choppin, G. R. M., Eds.; Dekker: New York, 1992; pp 157–207.

(4) Danesi, P. R.; Chirizia, R.; Coleman, C. F. The kinetics of metal solvent extraction. In *Critical Reviews in Analytical Chemistry*; Campbell, B., Ed.; CRC Press: Boca Raton, Florida, 1980; p 1.

(5) Ungaro, R.; Arduini, A.; Casnati, A.; Ori, O.; Pochini, A.; Ugozzoli, F. Complexation of ions and neutral molecules by functionalized calixarenes. In *Computational Approaches in Supramolecular Chemistry*; Wipff, G., Ed.; Kluwer Academic Publishers: Dordrecht, 1994; pp 277–300.

(6) Ungaro, R.; Casnati, A.; Ugozzoli, F.; Pochini, A.; Dozol, J.-F.; Hill, C.; Rouquette, H. *Angew. Chem., Int. Ed. Engl.* **1994**, *33*, 1506–1509.

(7) Casnati, A.; Pochini, A.; Ungaro, R.; Ugozzoli, F.; Arnaud, F.; Fanni, S.; Schwing-Weil, M.-J.; Egberink, R. J. M.; Reinhoudt, D. N. J. *Am. Chem. Soc.* **1995**, *118*, 2767–2777.

(8) Hill, C.; Dozol, J.-F.; Lamare, V.; Rouquette, H.; Tournois, B.; Vicens, J.; Asfari, Z.; Bressot, C.; Ungaro, R.; Casnati, A. Nuclear waste treatment by means of supported liquid membranes containing calixcrown compounds. In *Calixarenes 50th Anniversary: Commemorative Issue*; Vicens, J., Asfari, Z., Harrowfield, J., Eds.; Kluwer Academic Publishers: Dordrecht 1995.

(9) Asfari, Z.; Bressot, C.; Vicens, J.; Hill, C.; Dozol, J.-F.; Rouquette, H.; Eymard, S.; Lamare, V.; Tournois, B. Cesium removal from nuclear waste water by supported liquid membranes containing calix-bis-crown compounds. In *Chemical Separations with Liquid Membranes*; Bartsch, R. A., Way, J. D., Eds.; American Chemical Society: Washington, DC, 1996; pp 376–390.

(10) Schwing-Weil, M.-J.; Arnaud-Neu, F. *Gazz. Chim. Ital.* **1997**, *127*, 687–692.

(11) Pearlman, D. A.; Case, D. A.; Caldwell, J. C.; Ross, W. S.; Cheatham, T. E., III; Ferguson, D. M.; Seibel, G. L.; Singh, U. C.; Weiner, P. K.; Kollman, P. A. *AMBER4.1*; University of California: San Francisco.

(12) Cornell, W. D.; Cieplak, P.; Bayly, C. I.; Gould, I. R.; Merz, K. M.; Ferguson, D. M.; Spellmeyer, D. C.; Fox, T.; Caldwell, J. W.; Kollman, P. A. *J. Am. Chem. Soc.* **1995**, *117*, 5179–5197.

(13) Wipff, G.; Lauterbach, M. *Supramol. Chem.* **1995**, *6*, 187–207.

(14) Lauterbach, M.; Wipff, G. Liquid–liquid Extraction of Alkali Cations by Calix[4]crown Ionophores: Conformation and Solvent Dependent Na⁺/Cs⁺ Binding Selectivity: A MD FEP Study in Pure Chloroform and MD Simulations at the water/chloroform Interface. In *Physical Supramolecular Chemistry*; Echegoyen, L., Kaifer, A., Eds.; Kluwer Academic Publishing, Dordrecht, 1996; pp 65–102.

(15) Wipff, G.; Troxler, L. MD studies on the picrate ion in water and in a nonaqueous solvent: solvation, interactions with Li⁺, K⁺, Cs⁺ and the 18C6 K⁺ complex. In *1st European Conference on Computational Chemistry*; Bernardi, F., Rivail, J.-L., Eds.; AIP Press: Woodbury, New York, 1995; pp 325–336.

(16) Åqvist, J. *J. Phys. Chem.* **1990**, *94*, 8021–8024.

(17) Jorgensen, W. L.; Chandrasekhar, J.; Madura, J. D. *J. Chem. Phys.* **1983**, *79*, 926–936.

(18) Jorgensen, W. L.; Briggs, J. M.; Contreras, M. L. *J. Phys. Chem.* **1990**, *94*, 1683–1686.

(19) Berendsen, H. J. C.; Postma, J. P. M.; van Gunsteren, W. F.; DiNola, A. *J. Chem. Phys.* **1984**, *81*, 3684–3690.

(20) Chang, T.-M.; Dang, L. X. *J. Phys. Chem. B* **1997**, *101*, 10518–10526.

(21) Darden, T. A.; York, D. M.; Pedersen, L. G. *J. Chem. Phys.* **1993**, *98*, 10089.

(22) Wipff, G.; Engler, E.; Guibaud, P.; Lauterbach, M.; Troxler, L.; Varnek, A., *New J. Chem.* **1996**, *20*, 403–417.

(23) Lauterbach, M.; Engler, E.; Muzet, N.; Troxler, L.; Wipff, G. *J. Phys. Chem.* **1998**, *102*, 245–256.

(24) Troxler, L.; Wipff, G.; Harrowfield, J. *J. Phys. Chem.* **1998**, *102*, 2, 6821–6830.

(25) Schouten, A.; Kanters, J. A.; Poonia, N. S., *Acta Crystallogr.* **1990**, *C46*, 61–64.

(26) *Handbook of Chemistry and Physics, 76th Edition*, D. R. Lide Ed., CRC Press: U.S.A., Chapt 12; **1995–1996**.

(27) Schweighofer, K. J.; Benjamin, I. *J. Phys. Chem.* **1995**, *99*, 9974–9985.

(28) Straatsma, T. P.; McCammon, J. A. *Annu. Rev. Phys. Chem.* **1992**, *43*, 407–435.

(29) Kollman, P. *Chem. Rev.* **1993**, *93*, 2395–2417.

(30) Varnek, A.; Wipff, G. *J. Mol. Struct. (THEOCHEM)* **1996**, *363*, 67–85.

(31) Caldwell, J.; Kollman, P. A. *J. Am. Chem. Soc.* **1995**, *117*, 4177–4178.

(32) Sun, Y.; Caldwell, J. W.; Kollman, P. A., *J. Phys. Chem.* **1995**, *99*, 10081–10085.

(33) McDonald, I. R., *Mol. Phys.* **1972**, *24*, 391–401.

(34) Singer, J. V. L.; Singer, K. *Mol. Phys.* **1972**, *24*, 357–390.

(35) Hoheisel, C.; Lucas, K. *Mol. Phys.* **1984**, *53*, 51–67.

(36) de Leeuw, S. W.; Smit, B.; Williams, C. P. *J. Chem. Phys.* **1990**, *93*, 2704–2714.

(37) Scott, W.; Müller-Plathe, F.; van Gunsteren, W. F. *Mol. Phys.* **1994**, *82*, 1049–1062.

(38) Fincham, D.; Quirke, N.; Tildesley, D. J. *J. Chem. Phys.* **1986**, *84*, 4535–4546.

(39) Fincham, D.; Quirke, N.; Tildesley, D. J. *J. Chem. Phys.* **1987**, *87*, 6117–6119.

(40) Smit, B.; Esselink, K.; Hilbers, P. A. J.; van Os, N. M.; Rupert, L. A. M.; Szleifer, I. *Langmuir* **1993**, *9*, 9–11.

(41) Smit, B.; Hilbers, P. A. J.; Esselink, K.; Rupert, L. A. M.; van Os, N. M. *J. Phys. Chem.* **1991**, *95*, 6361–6368.

(42) Wallqvist, A. *Chem. Phys. Lett.* **1991**, *182*, 237–241.

(43) DeBolt, S. E.; Kollman, P. A. *J. Am. Chem. Soc.* **1995**, *117*, 5316–5340.

(44) Girault, H. H.; Schiffrin, D. J. Electrochemistry of liquid–liquid interfaces. In *Electroanalytical Chemistry*; Bard, A. J., Ed.; Dekker: NY, 1989; pp 1–141.

(45) Troxler, L.; Wipff, G. *Anal. Sci.* **1998**, *14*, 43–56.

(46) Beudaert, P.; Lamare, V.; Dozol, J.-F.; Troxler, L.; Wipff, G. *Solv. Extract. Ion Exch.* **1998**, *16*, 597–618.

(47) Berny, F.; Muzet, N.; Schurhammer, R.; Troxler, L.; Wipff, G. MD Simulations on ions and ionophores at a liquid–liquid interface: from adsorption to recognition. In *Current Challenges in Supramolecular Assemblies*; Tsoucaris, G., Ed.; Kluwer Academic Publishers: Dordrecht, 1998; pp 221–248.

(48) Berny, F.; Muzet, N.; Troxler, L.; Wipff, G. Simulations of liquid–liquid interfaces: a key border in supramolecular chemistry. In *Supramolecular Chemistry: Where are we? Where are we going?* NATO ARW, Lerici; Tsoucaris, G., Ed.; Kluwer Academic Publishers: Dordrecht, 1999. In press.

(49) Popov, A. N. Counterions and adsorption of ion-exchange extracants at the water/oil interface. In *The Interface Structure and Electrochemical Processes at the Boundary Between two Immiscible Liquids*; Kazarinov, V. E., Ed.; Springer-Verlag: New York, 1987; pp 179–205.

(50) Randles, J. E., *Discuss. Faraday Soc.* **1957**, *24*, 194–199.

(51) Ishikawa, Y.; Kunitake, T.; Matsuda, T.; Otsuka, T.; Shinkai, S. *J. Chem. Soc., Chem. Commun.* **1989**, 736–737.

(52) Rappoport, H.; Kuzmenko, I.; Kjaer, K.; Howes, P.; Bouwman, W.; Als-Nielsen, J.; Leiserowitz, L.; Lahav, M. *J. Am. Chem. Soc.* **1997**, *119*, 11211–11216.

(53) Sagert, N. H.; Lee, W.; Quinn, M. J. *Can. J. Chem.* **1979**, *57*, 1218–1223.

(54) Danesi, P. R.; Chiarizia, R.; Pizzichini, M.; Saltelli, A. *J. Inorg. Nucl. Chem.* **1978**, *40*, 1119–1123.

(55) Vandegrift, G. F.; Horwitz, E. P. *J. Inorg. Nucl. Chem.* **1977**, *40*, 1119–1123.

(56) Dei, L.; Casnati, A.; Nostro, P. L.; Baglioni, P. *Langmuir* **1995**, *11*, 1268–1272.

(57) Carlà, M.; Gambi, C. M. C.; Baglioni, P. *J. Phys. Chem.* **1996**, *100*, 11067–11071.

(58) Dei, L.; Casnati, A.; Nostro, P. L.; Pochini, A.; Ungaro, R.; Baglioni, P. *Langmuir* **1996**, *12*, 1589–1593.

(59) Nostro, P. L.; Casnati, A.; Bossoletti, L.; Dei, L.; Baglioni, P. *Colloids Surf. A* **1996**, *116*, 203–209.

(60) Lauterbach, M.; Wipff, G.; Mark, A.; van Gunsteren, W. F. *Gazz. Chim. Ital.* **1997**, *127*, 699–708.

(61) Benjamin, I. *Chem. Rev.* **1996**, *96*, 1449–1475. Michael, D.; Benjamin, I. *J. Phys. Chem. B* **1998**, *102*, 5145 and references cited therein.

(62) Torrie, G. M.; Valleau, J. P. *J. Electroanal. Chem.* **1986**, *106*, 69–79.

(63) Wilson, M. A.; Pohorille, A. *J. Am. Chem. Soc.* **1996**, *118*, 6580–6587.

(64) Laaksonen, A.; Kusalik, P. G.; Svishchev, I. M. *J. Phys. Chem. A* **1997**, *101*, 5910–5918.

(65) Schlenkrich, M.; Nicklas, K.; Brickmann, J. *Ber. Bunsen-Ges. Phys. Chem.* **1994**, *94*, 133–145.

(66) van Buuren, A. R.; Marrink, S.-J.; Berendsen, J. C. *Colloids and Surfaces* **1995**, *102*, 143–157.

(67) Cascales, J. J. L.; Torre, J. G. d. I.; Marrink, S. J.; Berendsen, H. J. C. *J. Chem. Phys.* **1996**, *104*, 2713–2720.

(68) Smit, B.; Hilbers, P. A. J.; Esselink, K. *Tenside Surf. Deterg.* **1993**, *4*, 287–294.

(69) Ferrario, M.; Haughney, M.; McDonald, I. R.; Klein, M. L. *J. Chem. Phys.* **1990**, *93*, 5156–5166.

(70) Chang, T.-M.; Peterson, K. A.; Dang, L. X. *J. Chem. Phys.* **1995**, *103*, 7502–7513.

- (71) Jorgensen, W. L.; McDonald, N. A.; Selmi, M.; Rablen, P. R. *J. Am. Chem. Soc.* **1995**, *117*, 11809–11810.
- (72) Sokhan, V. P.; Tildesley, D. J. *Faraday Discuss.* **1996**, *104*, 193–208.
- (73) Meng, E. C.; Kollman, P. A. *J. Phys. Chem.* **1996**, *100*, 11460–11470.
- (74) Kovacs, H.; Kowalewski, J.; Laaksonen, A. *J. Phys. Chem.* **1990**, *94*, 7378–7385.
- (75) Eblinger, F.; Schneider, H. J. *J. Phys. Chem.* **1996**, *100*, 5533–5537.
- (76) Conti, J. J.; Othmer, D. F.; Gilmont, R. *J. Chem. Eng. Data* **1960**, *5*, 301.
- (77) Smith, P. E.; van Gunsteren, W. F. Methods for Evaluation of Long Range Electrostatic Forces in Computations of Molecular Systems. In *Computer Simulations of Biomolecular Systems*; van Gunsteren, W. F., Weiner, P. K., Wilkinson, A. J., Eds.; ESCOM: Leiden, 1993; pp 182–212.
- (78) Luty, B. A.; Davis, M. E.; Tironi, I. G.; van Gunsteren, W. F. *Molecular Simul.* **1994**, *14*, 11–20.
- (79) Hautman, J.; Klein, M. L. *Mol. Phys.* **1992**, *75*, 379–395.
- (80) Berny, F.; Wipff, G. Unpublished results.
- (81) Chipot, C.; Wilson, M. A.; Pohorille, A. *J. Phys. Chem. B* **1997**, *101*, 782–791.
- (82) Karaborni, S.; Esselink, K.; Hilbers, P. A. J.; Smit, B.; Karthäuser, J.; van Os, N. M.; Zana, R. *Science* **1994**, *266*, 254–256.
- (83) Böcker, J.; Brickmann, J.; Bopp, P. *J. Phys. Chem.* **1994**, *98*, 712–717.
- (84) Shelley, J.; Watanabe, K.; Klein, M. *Int. J. Quantum Chem.: Quantum Biol. Symp.* **1990**, *17*, 103–117.
- (85) Watanabe, K.; Klein, M. L. *J. Phys. Chem.* **1991**, *95*, 4158–4166.
- (86) Smit, B.; Hilbers, P. A. J.; Esselink, K.; Rupert, L. A. M.; van Os, N. M.; Schlijper, A. G. *Nature* **1990**, *348*, 624–625.
- (87) Tarek, M.; Tobias, D. J.; Klein, M. L. *J. Phys. Chem.* **1995**, *99*, 1393–1402.
- (88) Wijmans, C. M.; Linse, P. *J. Phys. Chem.* **1996**, *11*, 12583–12591.
- (89) Smit, B. *Comput. Simul. Chem. Phys.* **1993**, 461–472.
- (90) Pohorille, A.; Wilson, M. A. *Origins Life Evolution Biosphere* **1995**, *25*, 21–46.
- (91) Marrink, S.-J.; Berendsen, H. J.-C. *J. Phys. Chem.* **1994**, *98*, 4155–4168.